INVESTIGATION OF THE PRODUCTION OF GAS PHASE ALUMINIUM IN RE-ENTRY

PR00123/D02 ISSUE 4

J BECK, I HOLBROUGH

Belstead Research Ltd.
387 Sandyhurst Lane
Ashford
UK
TN25 4PF

+44 1233 335054
info@belstead.com

Authorisation
Author: J Beck
Reviewer: I Holbrough
Issue: 4
Date: 17th April 2025

CONTENTS **PAGE NO**

LIST OF FIGURES

LIST OF TABLES

SUMMARY

This investigatory piece of work commissioned by the UKSA covers three areas, providing a starting point for the assessment of likelihood of, and mechanisms behind, the production of very small particulate phase aluminium which can potentially reside in the atmosphere for a long period of time.

The first part of the work is an assessment of the likelihood of significant vaporisation of aluminium from a range of particle sizes at different release altitudes. This work is performed using drag and heating algorithms which are standard in aerodynamic analyses and destructive re-entry tools. The work has found that there is a very high sensitivity to the particle surface properties. If an aluminium oxide particle is assumed, the vaporisation is low, whereas if the particles behave as aluminium objects with a thin oxide layer, then the vaporisation can be very significant. It is clear that more work is needed to understand this phenomena more clearly.

The second part of the work devised a set of plasma wind tunnel tests to investigate the relevant phenomena. The test plan is separated into two parts, a set of tests to evaluate the break-up of aluminium particles, and a set of tests to evaluate the vaporisation of the particles post break-up. The test geometries, required diagnostics and a set of preliminary conditions have been outlined. The parameters required to produce conditions which are representative of flight have been assessed and preliminary test matrices constructed for the two test aspects.

The final part of the work is a survey of relevant UK facilities which could be useful for the investigation of the emission production from spacecraft demise. This is a more general assessment, covering a wide range of hypersonic facilities, and it has been discovered that there are key facilities which are directly relevant to the investigation of the vaporisation of aluminium particles in re-entry. These facilities are the plasma torch at Oxford University and the light gas gun at the Open University. The set of devised tests have been adapted slightly to suit the capability of these facilities. This has allowed a two-stage 18 month programme to be proposed, which consists of a preliminary test campaign in each facility, where significant learning on how to conduct the tests effectively is expected, prior to testing to provide the data to support and enhance the analysis performed within the first part of this activity.

1 INTRODUCTION

Discussion with atmospheric chemists has highlighted that the key to the production of small aluminium particles (<1μm) is recondensation from the gas phase. Plasma wind tunnel tests demonstrate that aluminium particles shed in destructive re-entry tend to be large (100μm to 1cm), and are associated with minimal gas phase production in ground tests, evidenced by the minor aluminium emission spectroscopy signal. This investigation will assess what happens to these particles after release from the parent object. As they are small, they will decelerate very rapidly, but also heat very rapidly. As aluminium oxide is present in observation campaign spectrographic signals, such as Figure 1 from the AATV-1 re-entry, some vaporisation is expected.

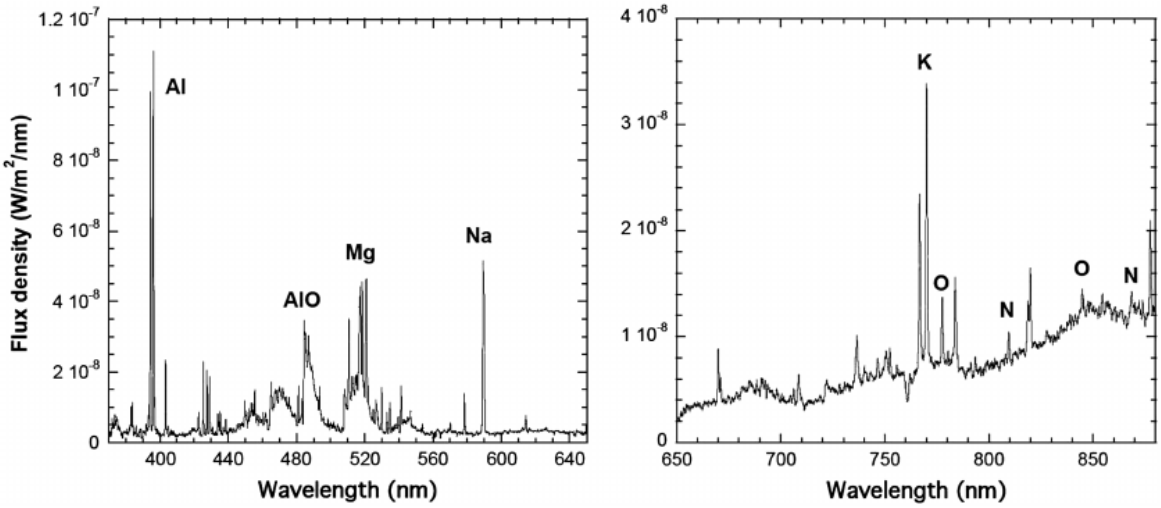

Figure 1: ATV-1 Emission Spectra

Consistent behaviour is shown from aluminium components in plasma wind tunnel demise testing. The separation of aluminium material from the bulk object is dominated by the behaviour of its oxide layer. This is demonstrated in Figure 2 where the aluminium housing of a small reaction wheel is seen to tear in a test performed within an ESA activity (1).

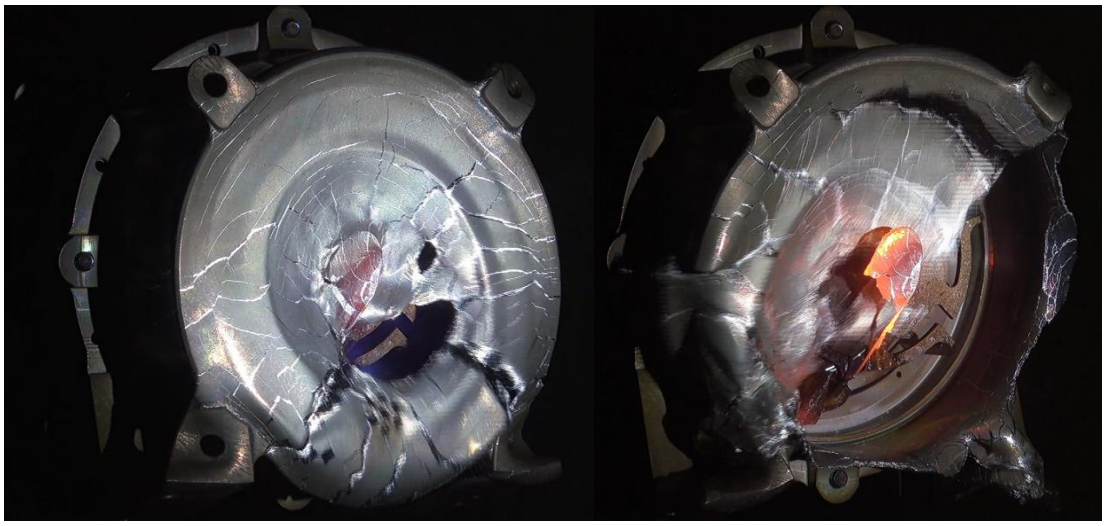

Figure 2: Failure of Aluminium Housing of Reaction Wheel in Wind Tunnel Test

The mechanism at play here is that there is a thick oxide layer on the aluminium surface, which contains the metal which has reached its melting point. As the metal melts, it becomes less resistant to the forces from the airflow, and the oxide-bound material begins to deform. This deformation eventually becomes sufficient that the oxide layer tears, which is evident in both Figure 2 images. The aluminium parts removed are very large, which is determined partially by the very high surface tension of molten metals, but mainly by the oxide layer behaviour. This suggests that the aluminium particle sizes produced by the melting of aluminium inside an oxide layer are actually quite large.

Released aluminium metal has been observed in wind tunnel testing within the EU ReDSHIFT activity (2). In Figure 3, a 4mm thick aluminium plate was heated in a plasma wind tunnel, and the aluminium was again observed to melt within the oxide layer to the extent that it began to flow downwards, still within the oxide layer, under gravity. Eventually, the mass of the molten material became sufficient that

the oxide layer tore, and molten aluminium was observed to escape. The escaping molten aluminium is observed at the bottom of the high-speed camera image, and could be seen to very rapidly form an oxide skin. Again, this is a relatively large aluminium fragment, a few centimetres long.

Figure 3: High Speed Camera Image Showing Release of Molten Metal Aluminium

This ‘particle’ size is consistent with the aluminium frame lost from a CubeSat within the same experimental campaign (2), as shown in Figure 4. It is possible that some small particles are produced in the tearing of the oxide layer, but it is clear that the vast majority of the mass resides in large particles.

Figure 4: Removal of Aluminium from CubeSat Frame in Wind Tunnel Test

Within the ATISPADE ESA study (3), a first attempt to estimate the particles sizes produced during re-entry was made. This was based on the idea that the large particles produced from the tearing of the oxide layer would undergo secondary break-up in the airstream. This is a reasonable hypothesis, and there are correlations that exist, but not for this particular flow regime. Importantly, these correlations do not account for the presence of the oxide layer, which would tend to drive towards larger particles being produced. This is revisited in Section 2.4, but the initial analysis suggested particles of some tens to hundreds of microns being produced, which are large enough to fall out of the atmosphere rapidly.

Once the particles are produced, they are still moving at high speed. However, due to their small size,

they will be rapidly decelerated, whilst being rapidly heated. This provides a potential mechanism for the production of gas phase aluminium, or more likely aluminium oxide from the particle surface, which can then recondense into the sub-micron particles of interest. The question then becomes whether the particles slow down before significant heating occurs, in which case there is little gas phase aluminium produced, or whether the particles are able to vaporise significantly before they decelerate to the point where the heating shuts off. This is likely to depend on the size of the particle and the altitude at which it is produced.

The first part of this study investigates the likelihood of the production of aluminium oxide vapour which can then recondense into small particles. This is a theoretical investigation based on state-of-the-art engineering assessments which are used to calculate demise and casualty risk in re-entry. The output of this investigation will then be used to construct a test plan to explore the key phenomena in order to provide more confidence in the results obtained. The intention is to perform these tests at a plasma wind tunnel, a facility which is not currently available in the UK. A survey of facilities that can contribute to the understanding of the environmental impact of spacecraft demise is planned.

2 MAPPING VAPORISATION POTENTIAL OF ALUMINIUM PARTICLES PRODUCED IN RE-ENTRY

2.1 Re-Entry Conditions

The conditions which will be experienced by particles of aluminium that break-off a re-entering spacecraft will be determined by the nature of the re-entry, and the ballistic coefficient of the fragment.

Four cases will be considered. These cover two ballistic coefficients, one (100kg/m^2) which is representative of a satellite with solar arrays, and a higher value (250kg/m^2) which is at the upper end associated with upper stages, as calculated in (4). Each ballistic coefficient is considered on two trajectories – one a decaying circular orbit, and the other typical of a controlled re-entry from a 750km orbit. The importance of the trajectories is to provide the velocities of the spacecraft at which the particles are released, as this forms the initial condition for the particle heating and deceleration.

The velocities in the 100km to 50km altitude window of interest are shown in Figure 5. The speed in the higher part of the trajectory is driven by the re-entry type, but below 85km, the ballistic coefficient takes over, and by 60km, the velocity is driven primarily by the object ballistic coefficient. It is worth noting that these velocities are the maximum values at which the particles will be released as fragmentation of the spacecraft results in smaller, lower ballistic coefficient objects, which decelerate more rapidly. As such, these velocities form a sensible conservative assessment of the release conditions.

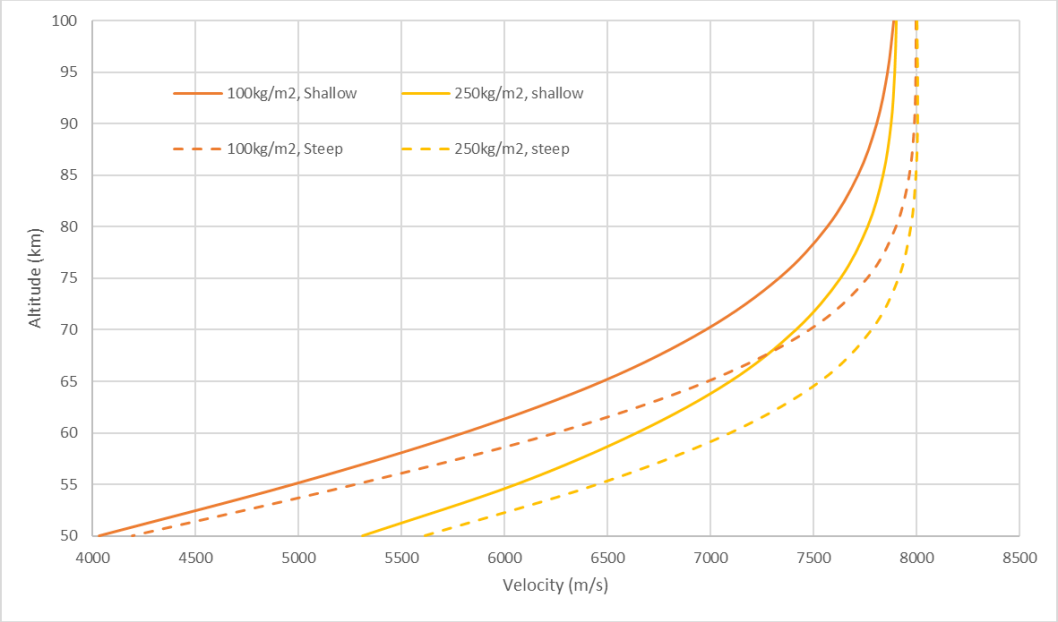

Figure 5: Spacecraft Velocities in Re-entry

The deceleration of particles will be sufficiently fast that no significant change in altitude is expected during the deceleration phase to be assessed here. This means that a constant atmospheric density can be assumed for each altitude condition, simplifying the analysis. The density as a function of altitude used in this work is given in Table 1, and is consistent with the US76 standard atmosphere model. The variation in density across the altitudes of interest is over four orders of magnitude.

Altitude (km)	Density (kg/m^3)
100	5.65e-7
95	1.35e-6
90	3.40e-6
85	8.22e-6
80	1.85e-5
75	4.05e-5
70	8.30e-5
65	1.62e-4
60	3.11e-4
55	5.69e-4
50	1.02e-3

Table 1: Atmospheric Density Model

2.2 Particle Model

In order to keep the model relatively simple, the particles are assumed to be spherical in shape. This provides a good first assessment of the heating and drag, allowing the balance between heating and deceleration to be determined. Five sizes of particle are considered, from 1mm to 30µm in diameter. As these particles are very small, their length scales are closer to the length scales of the mean free path than would be the case for spacecraft objects. This results in the flow around these particles being more rarefied. As this makes a significant difference to both the drag and the heating, increasing it in both cases, it is important that the rarefied nature of the flow is properly accounted for. This is done using the Knudsen number,

$$Kn = \frac{\lambda}{L}$$

where λ is the mean free path and L is the diameter of the particle. The mean free path, which is the mean distance between molecular collisions is calculated using the hard sphere approximation as

$$\lambda = \frac{1}{\sqrt{2}\pi d^2 n}$$

where d is the atomic diameter (taken as 3.6e-10m on average for air) and n is the number density, which is calculated from the atmospheric density, ρ, as

$$n = \frac{\rho}{RA}$$

where R is the average relative molecular mass of air (28.9kg/kmol) and A is Avogadro's number (6.02e26kmol^{-1}). The drag coefficient is then bridged between the free molecular value (C_{df} =2.0) and the continuum value (C_{dc} =0.92) using

$$C_d = aC_{df} + (1-a)C_{dc}$$

where

$$a = \frac{Kn}{0.1 + Kn}$$

The drag is given by

$$D = \frac{1}{2}\rho V^2 C_d A$$

where A is the projected area of the sphere and V is the velocity.

The heat flux to the particle is again split between free molecular and continuum contributions in order to account for the rarefied flow. The free molecular heating at the stagnation point is

$$q_f = \frac{1}{2}\rho V^3$$

which is applied to the whole surface of the particle using a shape factor of 0.25 to account for the ratio of the projected to total surface areas. The continuum heating is given by the Detra-Kemp-Ridell stagnation point formula,

$$q_c = \frac{9817750\sqrt{\frac{\rho}{1.2252}}}{\sqrt{\frac{L}{0.6096}}}\left(\frac{v}{3048}\right)^{3.15}$$

which is then applied to the whole spherical surface using a shape factor of 0.23. To obtain the rarefied heating, an exponential bridging function

$$q = \frac{1}{\frac{1}{q_c} + \frac{1}{q_f}}$$

is used. There are a number of heating bridging functions in use, and this is the default for most objects as used in both SAMj and DRAMA.

The particles are assumed to have an initial temperature of 850K, which is the melt temperature of aluminium alloys used in spacecraft. There are two other important parameters for the assessment of the heating of the particles. The emissivity is taken as 0.8 as this is consistent with oxidised surfaces of most metals and most ceramic materials. Some care is needed here, as post wind tunnel test measurements of aluminium surface yield a lower, 0.4, value. Ceramic surfaces are also low catalycity to the recombination of oxygen atoms at the surface, which reduces the heat flux input. The first analysis uses a 40% heat flux reduction for this effect. Again, some care must be taken, as oxide layers on contiguous aluminium objects show a higher catalycity. Sensitivity to both these aspects will be investigated.

2.3 Basic Drag and Heating Assessment

Two cases are considered in this part of the assessment, with the differences being the catalycity and emissivity of the particle surfaces. The two different cases are shown in Table 2. The particles are primarily expected to be driven by aluminium oxide properties, which suggests a high emissivity and a low catalytic recombination of oxygen atoms at the surface. Both of these tend to reduce the heating of the particles, the former by a high radiative rejection of heat, and the latter by the surface not gaining the bond heat energies from the molecular recombination reactions.

Case	Catalycity	Emissivity	Comments
1	0.6	0.8	Aluminium oxide material properties
2	1	0.4	Behaviour of oxidised aluminium surface in tests

Table 2: Catalycity/Emissivity Cases

It is worth noting, however, that the behaviour of solid aluminium parts in wind tunnel tests, which are larger, but have an oxidised surface, display different behaviour. In this case, the emissivity is significantly lower, thus reducing the rejected heat, and the catalycity promotes full recombination of the molecules. This subjects the particle surface to a much higher heat flux, and thus can be considered a worse case for the production of vapour. The higher catalycity is suggested by Park et al. (4) to be a function of the roughness of the particle surface, which they investigated experimentally.

It is assumed that the particles do not remain in the wake of the object from which they are ejected, and that they encounter quiescent air. The heating to particles will be significantly reduced in the wake as the relative velocity with the air is reduced, and this is the primary driver of the aerothermodynamic heating.

2.3.1 Drag Timescales

The drag timescales are highly dependent upon the atmospheric density and the particle size. At 100km, the timescales are of the order of a few tens of seconds, as shown in Figure 6. The difference in drag for the larger and smaller particles is evident, with the smallest particles slowing down much more rapidly.

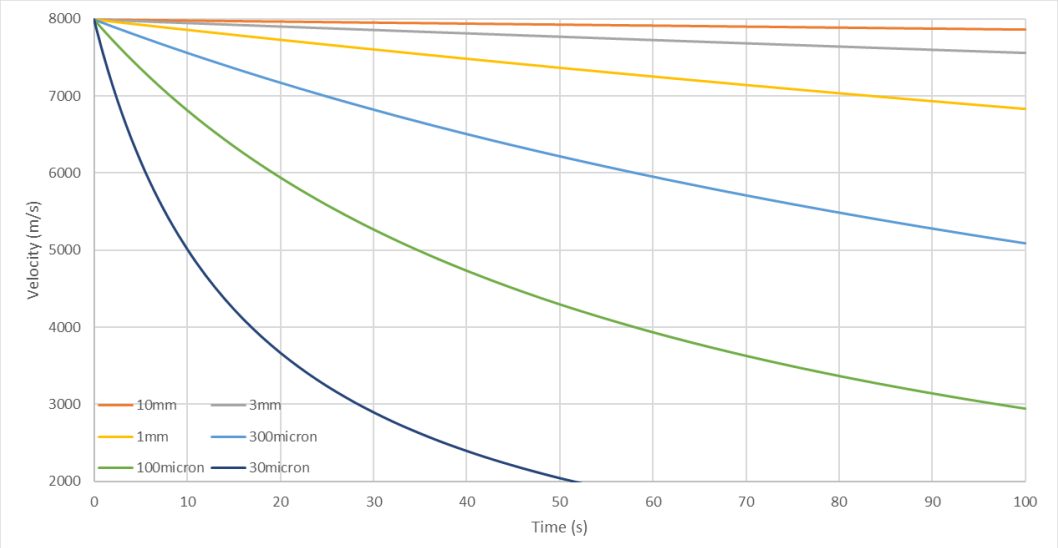

Figure 6: Drag Timescales at 100km (Standard, Shallow)

At 75km, the drag timescales have reduced to the order of 1s, as shown in Figure 7. This is driven by the higher density of the atmosphere at this altitude.

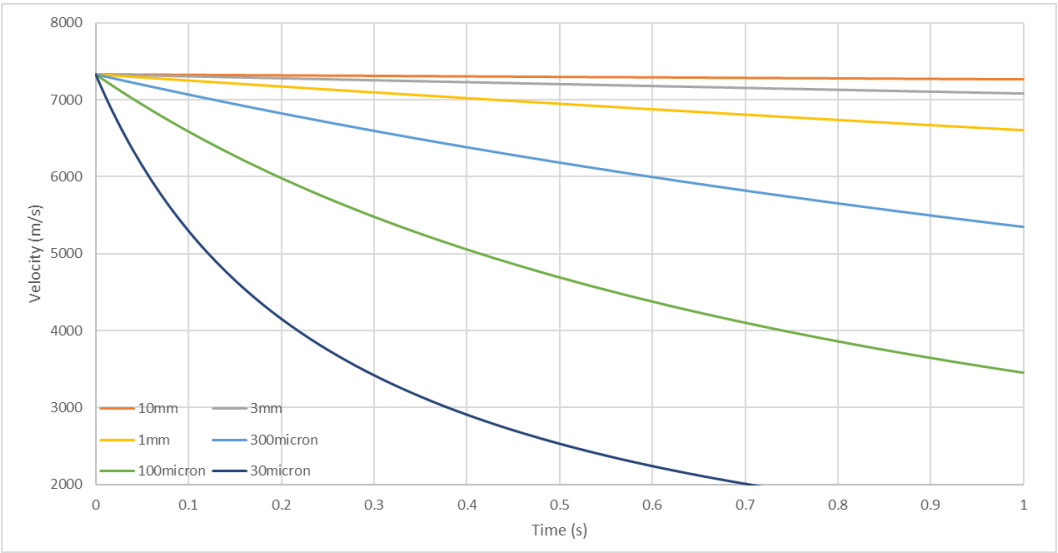

Figure 7: Drag Timescales at 75km (Standard, Shallow)

This is reduced to the order of tenths of seconds by 50km altitude, as shown in Figure 8.

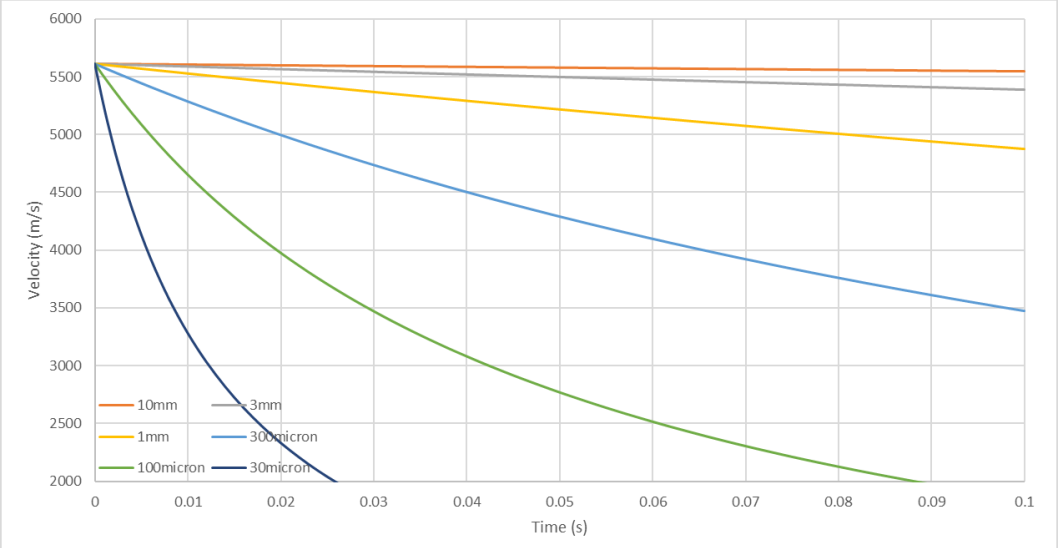

Figure 8: Drag Timescale at 50km (High Ballistic Coefficient, Steep)

This demonstrates that the time of interest for vaporisation of particles is very short indeed, and that the rapid heating in this period is critical to the particle temperatures which can be achieved.

2.3.2 Aluminium Oxide Property Particles

2.3.2.1 Heating Variation with Altitude

This analysis is performed with the aluminium oxide properties (low catalycity), standard ballistic coefficient and the shallow trajectory. In this case, the heating of the particles does not become significant until lower altitudes are reached. The temperatures reached by the different sized particles when released at 90km altitude are shown in Figure 9. The maximum temperature is approximately half the melt temperature of aluminium oxide. This suggests that even for the smallest particles likely to be produced in aluminium demise, there is likely to be little vaporisation.

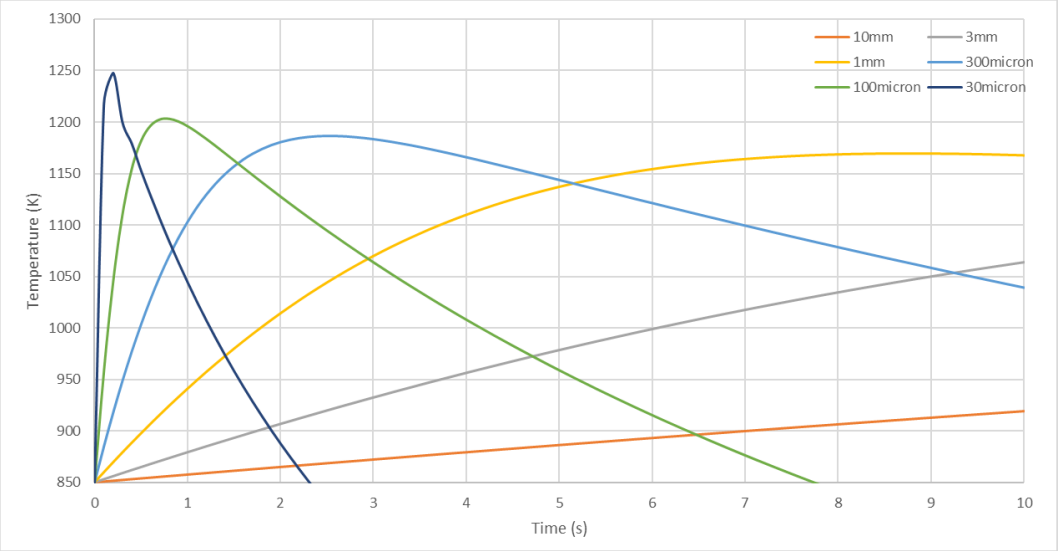

Figure 9: Particle Heating at 90km (Standard, Shallow)

Reducing the altitude to 80km gives the results in Figure 10. Here the temperatures are becoming significantly higher, but the oxide melt temperature (2327K) is still not reached. It is worth noting that

the amount of time spent at the higher temperatures is also reducing significantly.

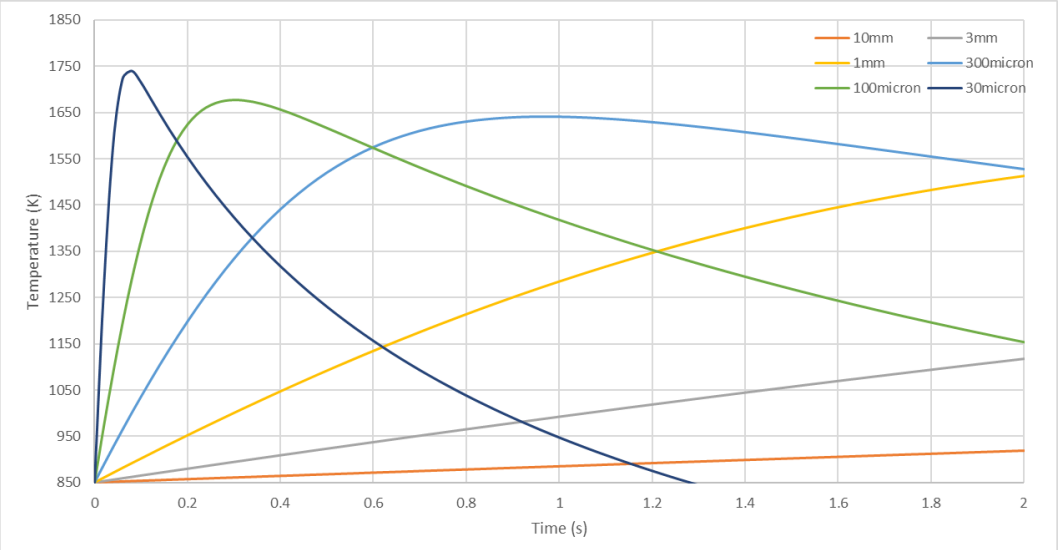

Figure 10: Particle Heating at 80km (Standard, Shallow)

Satellite fragmentation is usually considered to take place at approximately 78km, although this has only been observed on controlled re-entries which are inherently steeper. The shallow trajectories which are experienced in uncontrolled re-entry from a decaying circular orbit tend to show a higher heat soak, and it is generally thought that this will result in an earlier spacecraft fragmentation somewhere around 85km. The major demise phase of satellites begins at this altitude, and tends to run to somewhere between 60km and 70km, with the majority of the aluminium objects demising by 70km.

Reducing the altitude to 75km, which is a critical part of the re-entry for demise, gives the result shown in Figure 11. The temperatures here are higher, and suggest that particles of 1mm diameter and below can be of interest as they reach temperatures above 1500K, although this is not necessarily sufficiently hot for significant vaporisation to occur.

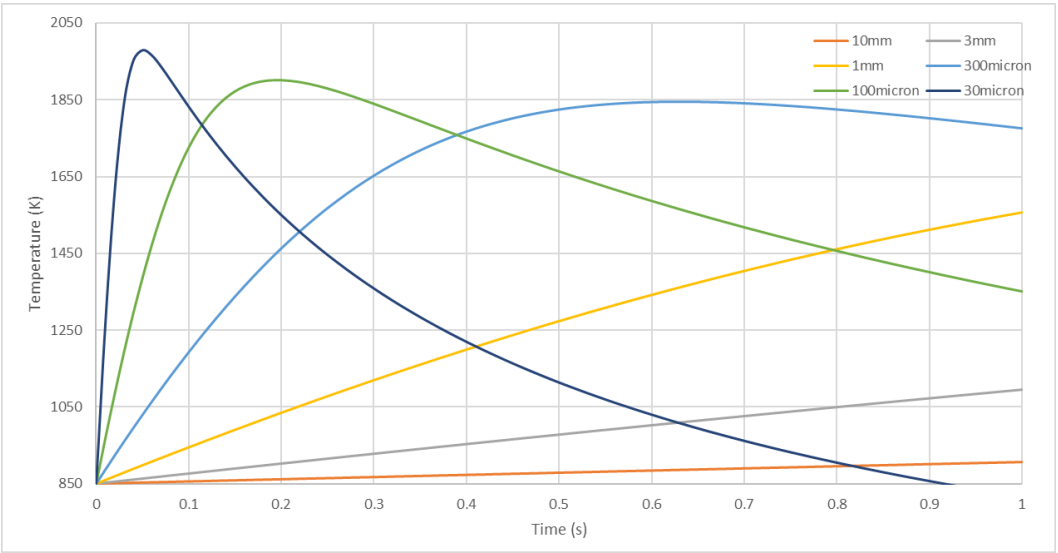

Figure 11: Particle Heating at 75km (Standard, Shallow)

Continuing in the critical part of the trajectory, the heating at 70km is shown in Figure 12. The temperatures reached further increase, but the oxide melt temperature is still to be achieved. As most of the particles are expected to be relatively large, this suggests that for an uncontrolled re-entry of a standard spacecraft with a moderate ballistic coefficient, there is limited vaporisation of aluminium oxide particles. Some vaporisation is likely to occur at these temperatures, which will be assessed in Section 2.5.

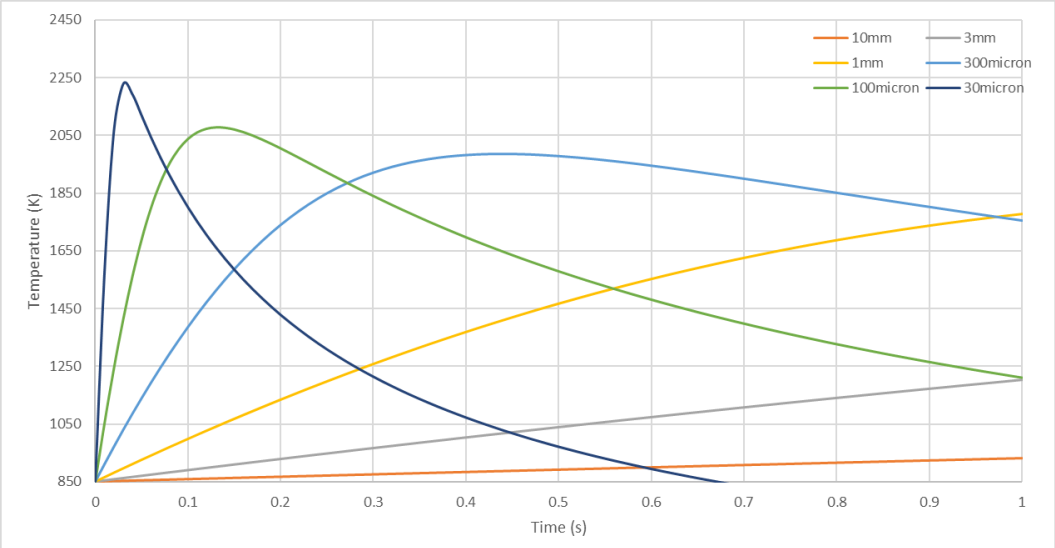

Figure 12: Particle Heating at 70km (Standard, Shallow)

By 60km, the peak temperatures are similar, but the timescale is shorter, as shown in Figure 13. This supports the assertion that vaporisation on this trajectory is limited, unless significant vaporisation occurs below the oxide melt point.

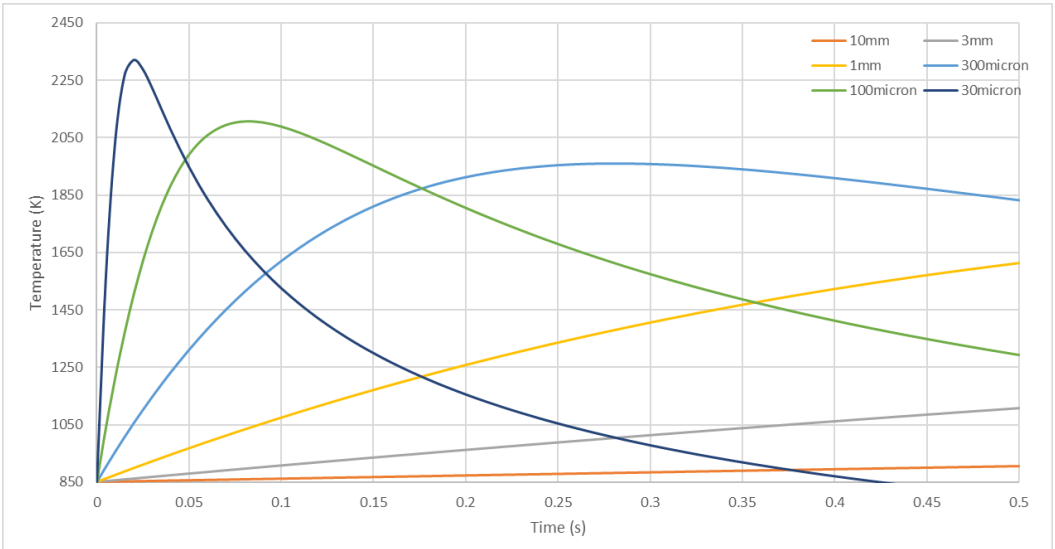

Figure 13: Particle Heating at 60km (Standard, Shallow)

Finally, for the standard ballistic coefficient, shallow trajectory, Figure 14 shows the heating at 50km. Here, the spacecraft has slowed sufficiently that the heating is much slower, such that the maximum particle temperatures are reduced. This is consistent with the general finding that very little demise occurs below this altitude on a shallow trajectory.

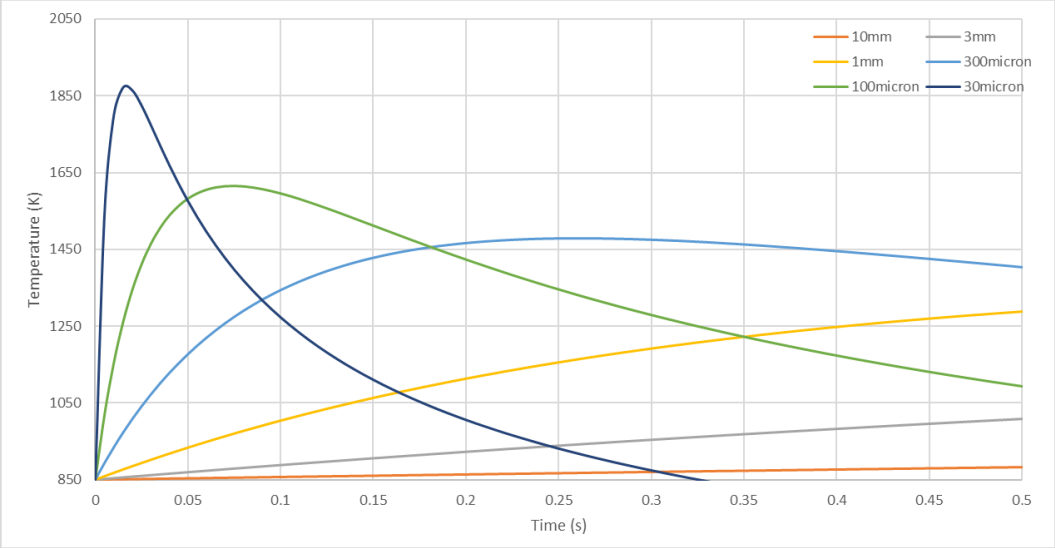

Figure 14: Particle Heating at 50km (Standard, Shallow)

2.3.2.2 Impact of Spacecraft Ballistic Coefficient on Heating

The assessment of the previous section suggests that the primary interest lies in the smaller particles. Therefore, for the assessment of the trajectory impact, only the sub-millimetre particles will be considered. This allows comparison of the trajectories without overcomplicating the figures.

At 80km, there is a small impact of the ballistic coefficient, as shown in Figure 15. The deceleration from drag is low at this stage as the atmosphere is thin, resulting in a small difference in the velocity, which drives the increase in the temperatures.

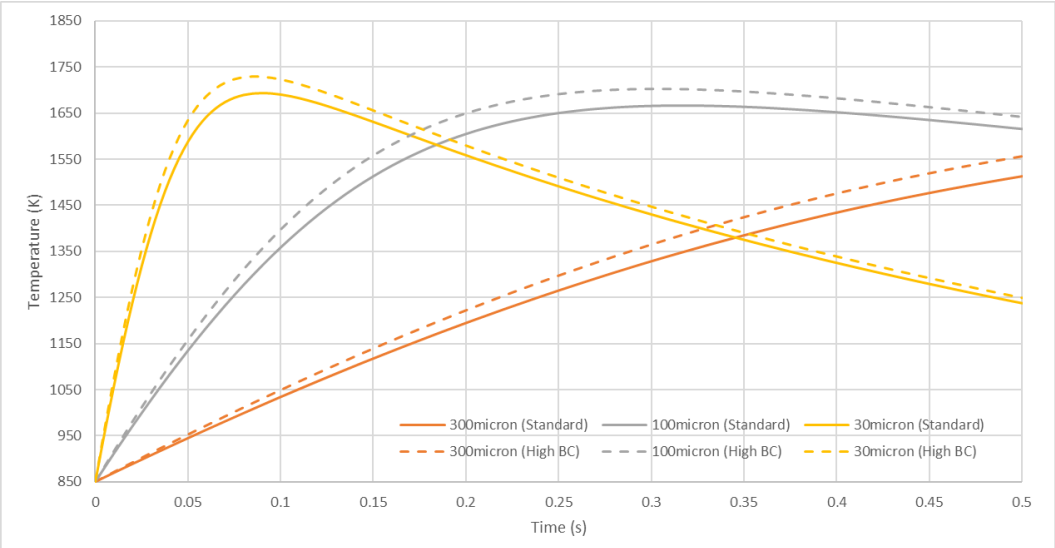

Figure 15: Ballistic Coefficient Effect at 80km

The increase in the particle temperatures is more significant at 70km, as shown in Figure 16. All three particle sizes are now reaching above 2000K.

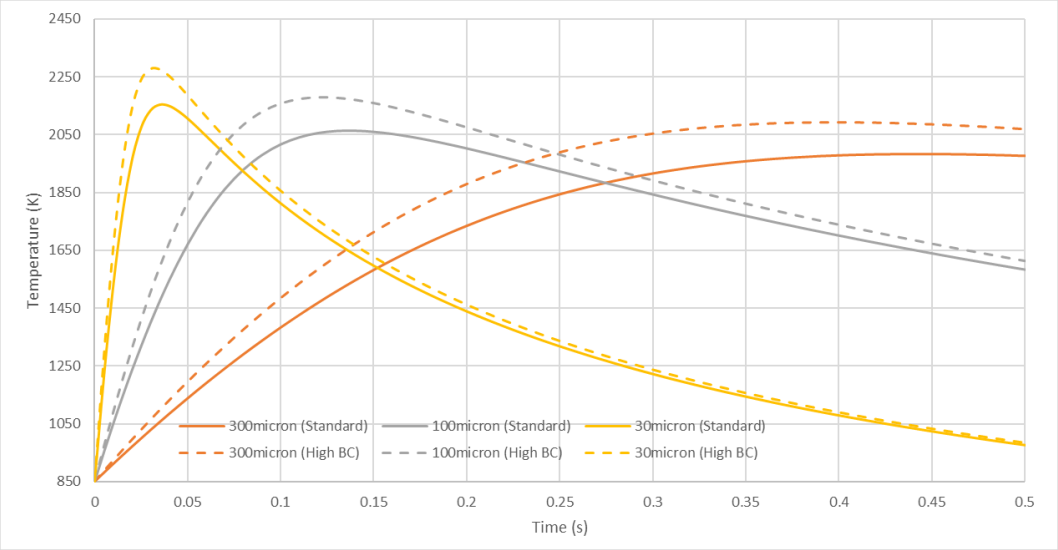

Figure 16: Ballistic Coefficient Effect at 70km

This trend continues at 60km, as shown in Figure 17. This is the first simulation which suggests a particle temperature above the oxide melt temperature. Indeed, this is suggested for the two smallest particle sizes.

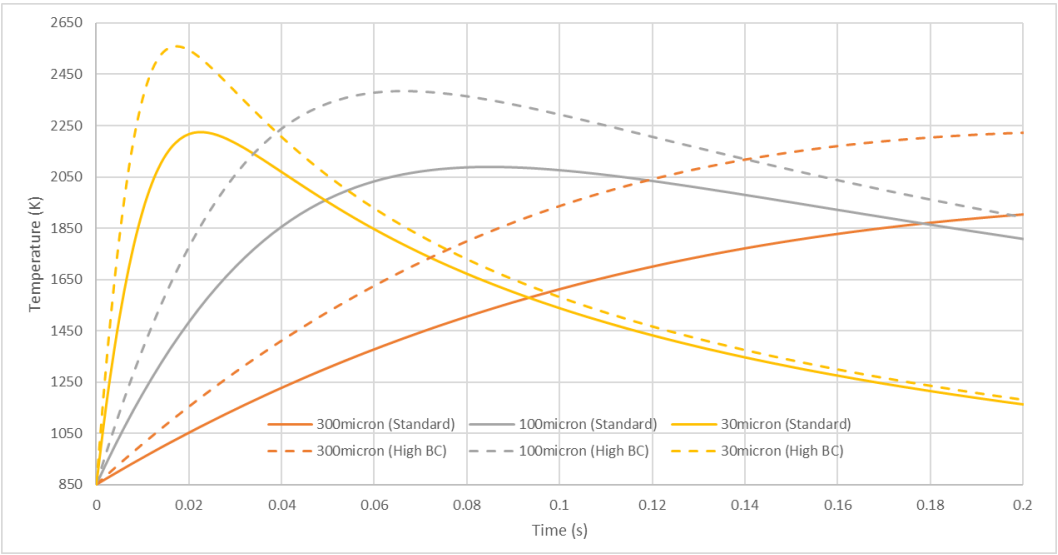

Figure 17: Ballistic Coefficient Effect at 60km

Although the difference at 50km, is again greater, the maximum temperatures are lower, which suggests that the emission peak will be above this altitude. Importantly, it is expected that demise will essentially be complete by this altitude on an uncontrolled, shallow re-entry.

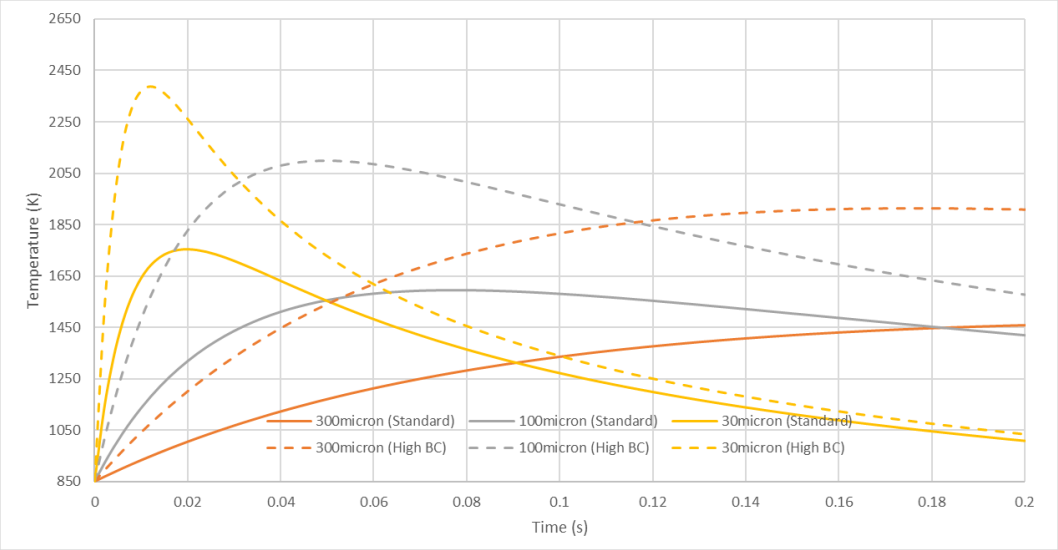

Figure 18: Ballistic Coefficient Effect at 50km

This analysis confirms that the primary altitudes of interest are relatively low, between 60km and 80km, for uncontrolled re-entries, and that the potential for emissions is increased with the ballistic coefficient of the re-entering object.

2.3.2.3 Impact of Trajectory Type on Heating

Figure 5 shows that the velocity of a re-entering spacecraft is affected by the trajectory type, such that the velocities are higher at given altitudes for direct re-entries. The effect is smaller than that seen from the ballistic coefficient, particularly at lower altitudes. The major difference between the trajectory types is that the steep, controlled, re-entry is much shorter. This means that the heating of the spacecraft is reduced, so less of the spacecraft is demised, and what demise does occur tends to occur at lower altitudes. Therefore, these trajectories are of particular interest as the particle generation at 50km to 60km altitudes is likely to be higher, and this is suggested to be the altitudes of most interest for aluminium oxide vaporisation.

This assessment is performed initially using the standard ballistic coefficient object, and the impact at 80km, 70km and 60km is shown in Figure 19 to Figure 21. The effect is noticeable, but does not increase as the altitude decreases.

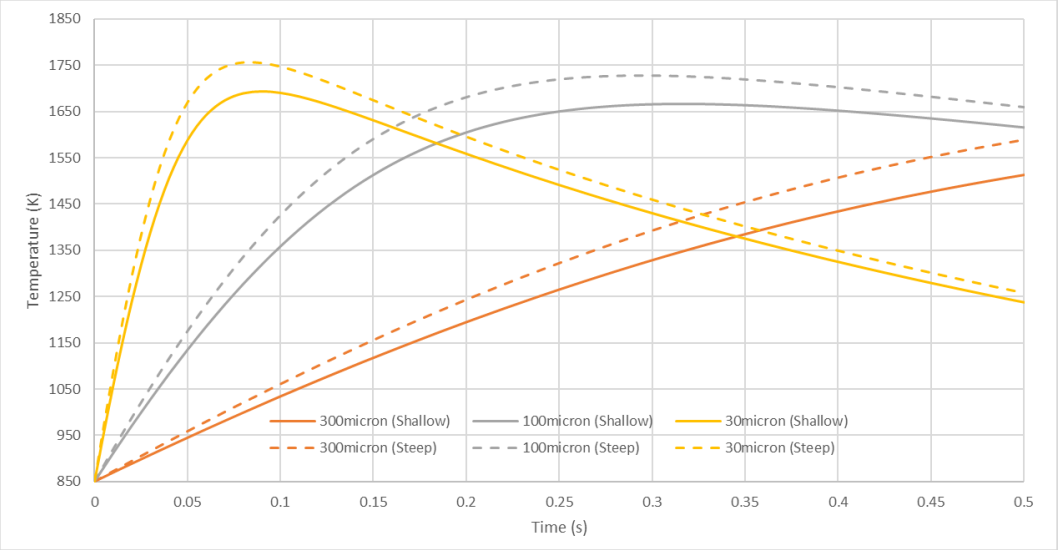

Figure 19: Trajectory Impact at 80km

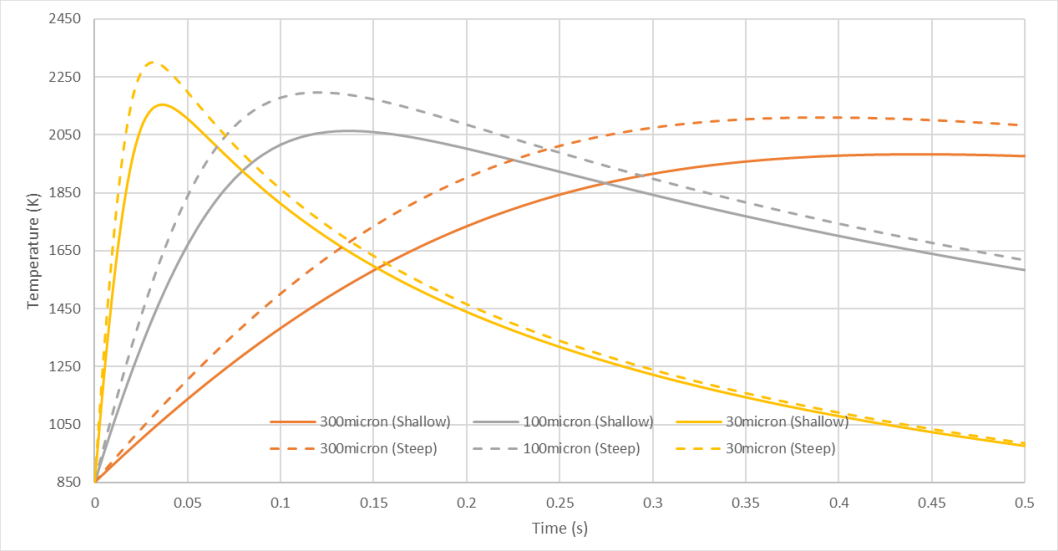

Figure 20: Trajectory Impact at 70km

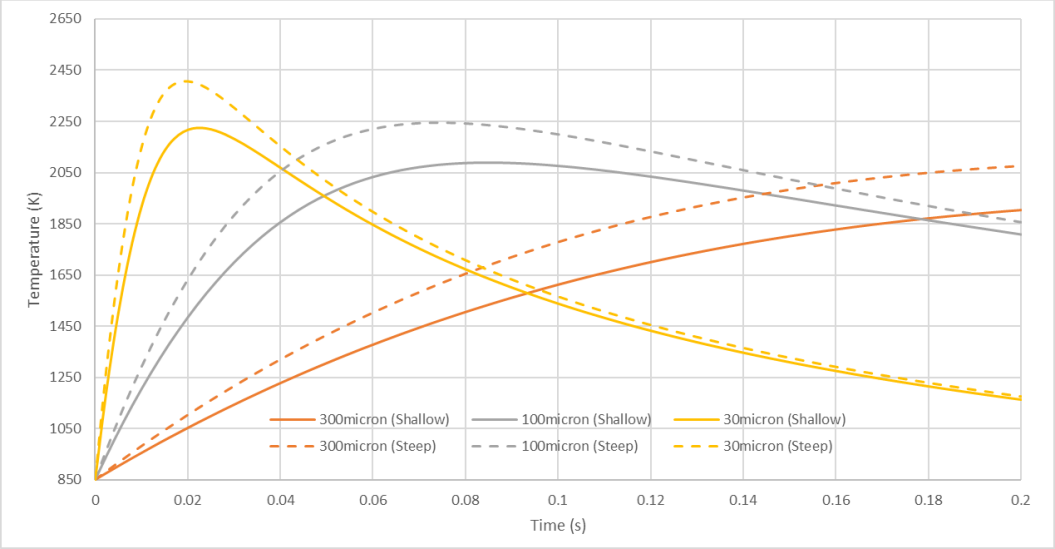

Figure 21: Trajectory Impact at 60km

As mentioned previously, this analysis underplays the impact of the steep trajectory as the highest particle heating is obtained between 50km and 60km. Shallow re-entries are unlikely to have any significant demise below 60km, whereas this is much more likely for steeper re-entries.

Figure 5 suggests that the worst case is a high ballistic coefficient object on a steep trajectory. The trajectory effect on the high ballistic coefficient object is shown at 60km in Figure 22. This shows a further increase in the achievable particle temperatures, confirming this expectation.

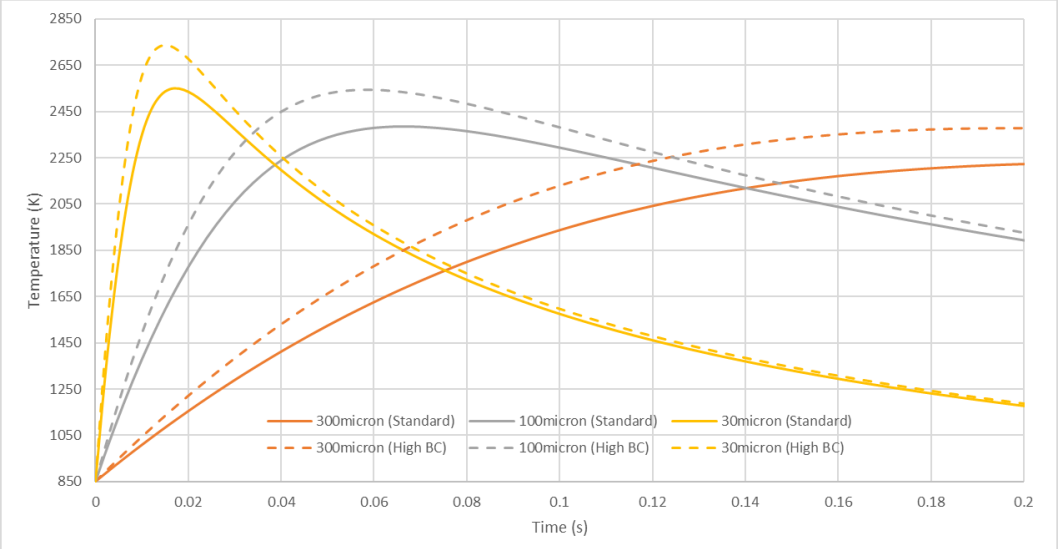

Figure 22: Trajectory Impact on High Ballistic Coefficient Object at 60km

2.3.3 Particles with Oxidised Aluminium Surface Property

2.3.3.1 Heating Variation with Altitude

The analysis is repeated using the surface properties obtained from testing for oxidised aluminium surfaces. The values are shown in Table 2, and result in halving the radiative emission at a given temperature, and almost doubling the incoming heat flux. Both of these changes will result in significantly higher heating of the particles, and as such, this provides a sensible worst case for the heat transfer.

As with the aluminium oxide particles, the shallow trajectory for a standard ballistic coefficient spacecraft is used for the baseline assessment. The smallest particles do not reach 2000K at an altitude of 85km, but this is passed by the time that 80km is reached, as shown in Figure 23.

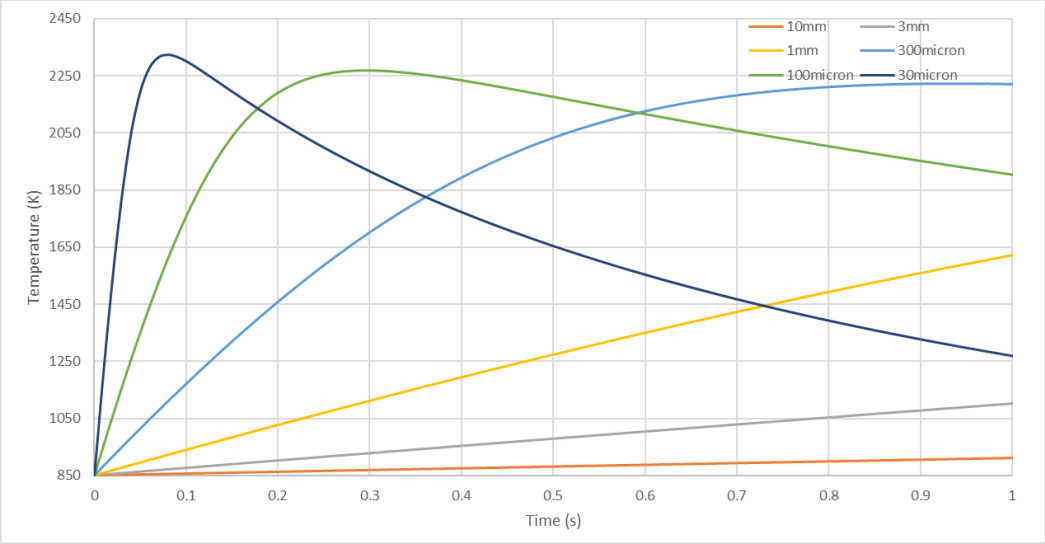

Figure 23: Particle Heating at 80km

The temperatures reached here are close to the oxide melt temperature. Comparison, for the three smallest particle sizes, with the aluminium oxide model, is shown in Figure 24. The difference is clear, and this model would suggest significantly more particulate vaporisation. Experimentation suggests that it is the catalycity which has the major effect, as the emissivity is highly temperature dependent and is offset by only a few degrees increase in temperature.

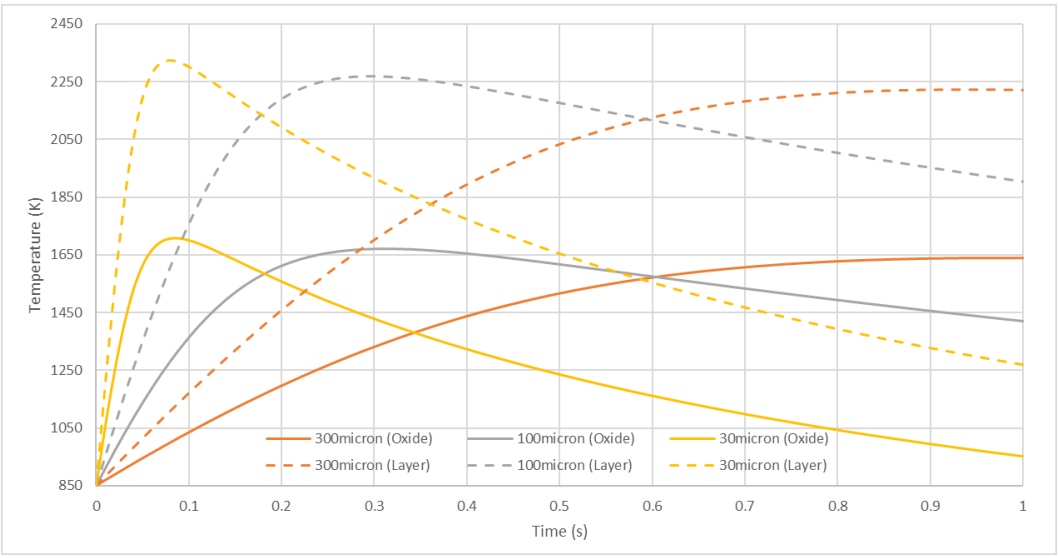

Figure 24: Impact of Surface Properties Model at 80km

Given this, this moves the potential for vaporisation for a standard satellite on an uncontrolled re-entry to higher altitudes, and makes the likelihood of observing significant vaporisation from such a re-entry much higher.

Similar plots at 75km and 70km are shown in Figure 25 and Figure 26. The temperatures are well above the melt temperature of the oxide.

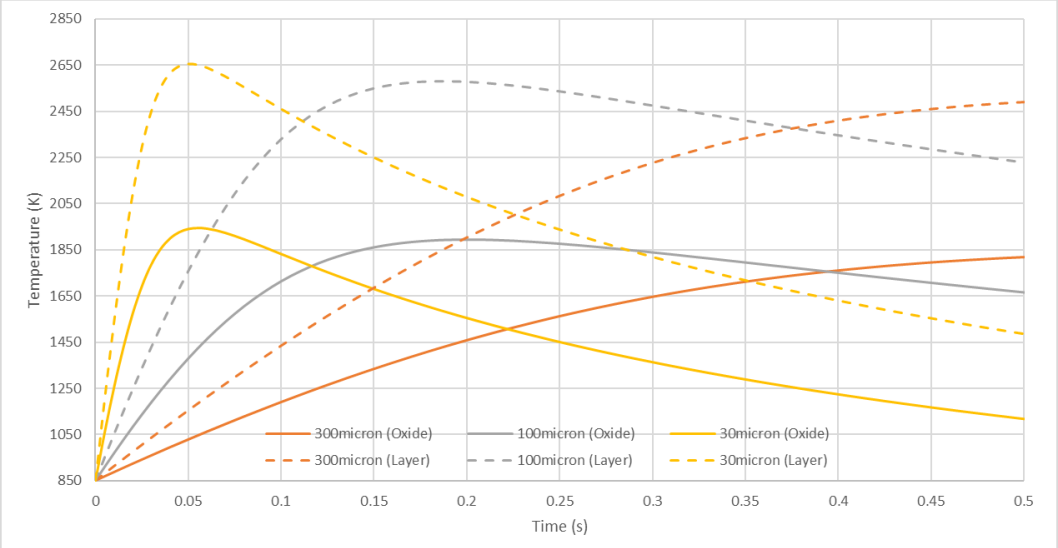

Figure 25: Impact of Surface Properties Model at 75km

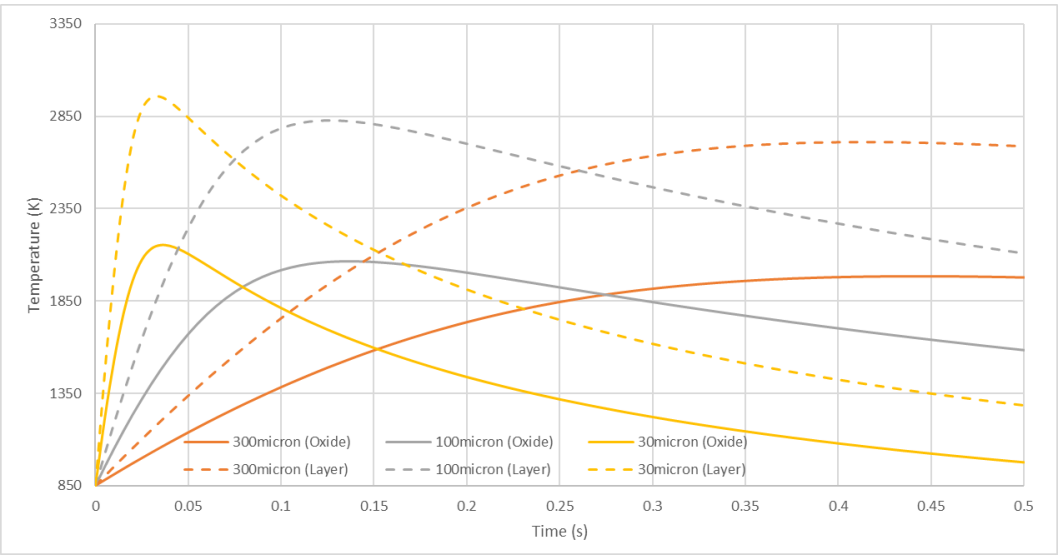

Figure 26: Impact of Surface Properties Model at 70km

Of interest here is that the 1mm particles also become hot, above 2300K, which was not seen for the aluminium oxide model. This is shown in Figure 27.

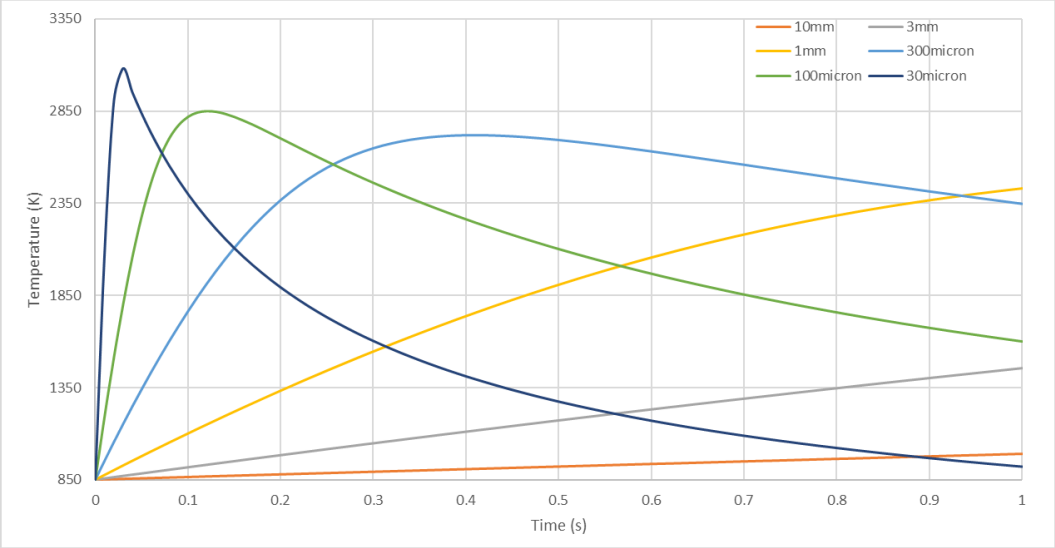

Figure 27: Particle Heating at 70km

For completeness, the particle heating at 60km and 50km is shown in Figure 28 and Figure 29. Here, the smallest particles approach the boiling temperature of aluminium oxide, suggesting vaporisation is likely. As with the aluminium oxide surface properties model, the heating is reduced at 50km as the spacecraft has slowed.

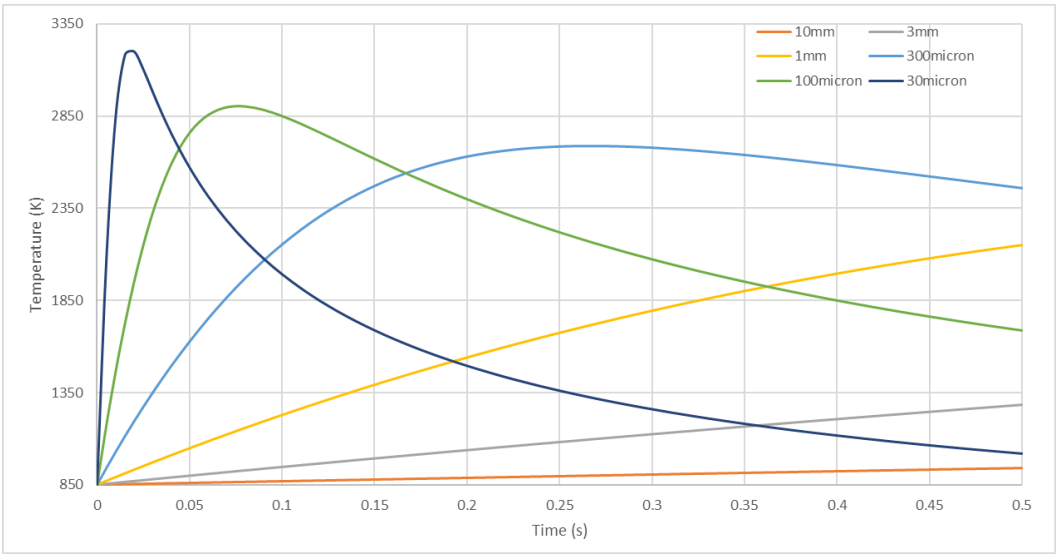

Figure 28: Particle Heating at 60km

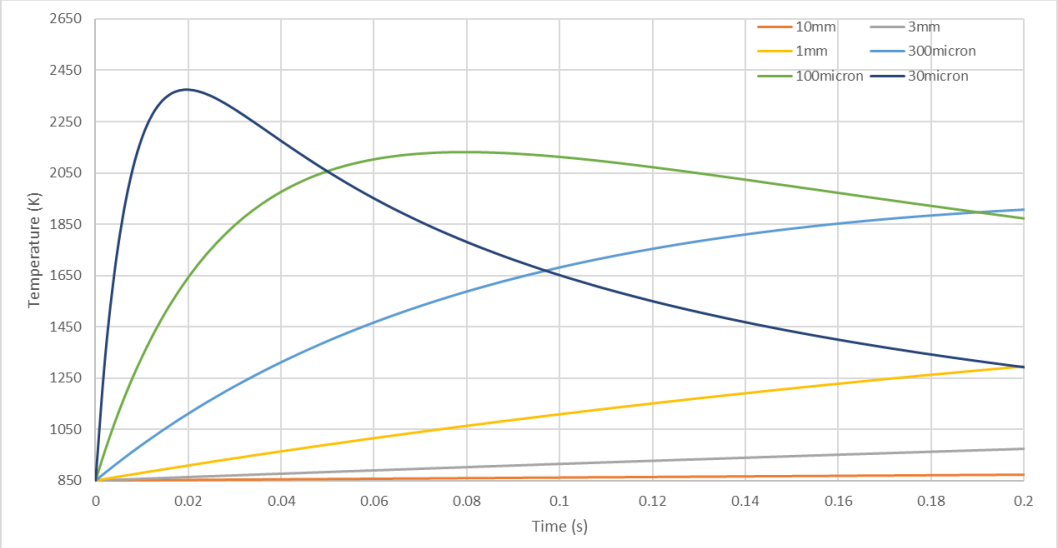

Figure 29: Particle Heating at 50km

It is clear from this analysis that the aluminium oxide layer behaviour as observed in the wind tunnel will make a significant difference to the potential vaporisation of aluminium oxide in re-entry. Where the surface properties match those observed for large scale aluminium parts, significantly more material can be expected to be vaporised.

2.3.4 Heating Summary

The heating analysis has shown that smaller particles reach significantly higher temperatures than larger particles, and that the highest temperatures occur around 60km altitude for a standard uncontrolled re-entry. Increase of the ballistic coefficient of the spacecraft can increase the heating to the particles at lower altitudes, but this is dependent upon the spacecraft remaining intact until quite late in the trajectory, or the fragments which produce particles having similarly large ballistic coefficients.

The surface properties have also been shown to have a significant impact on the temperatures which can be achieved. If the particles behave as aluminium objects with an oxide skin, then the heating received will be much higher, and there is likely to be some vaporisation above 75km. If they behave like a pure aluminium oxide material, then the heat received is reduced, and the vaporisation from an uncontrolled re-entry may be quite limited. It is worth noting that smaller particles are more likely to behave as aluminium oxide than larger particles, which could, at least in part, offset the temperature differences observed with particle size. It is worth noting that the particle surfaces are unlikely to be smooth, and this may drive the surface properties towards a higher catalycity, and thus being heated more.

This analysis shows that the temperatures reached are likely to be sufficient to display some vaporisation of aluminium oxide, which is consistent with the ATV-1 observations.

2.4 Droplet Break-up Assessment

The next part of this investigation revisits the work done within the ATISPADE (3) activity on the possible break-up of particles after release from a melting aluminium component. This work assumes again that the particles are emitted into the freestream, and do not reside in the wake of a larger component,

where the break-up and the heating will be significantly reduced.

The process of relatively large liquid droplets undergoing a secondary breakup, which is the most likely phenomenology of the particulate producing emissions from the above discussion, is well studied in the field of sprays for droplets. This analysis is generally restricted to conditions where the density ratio between the liquid and gas phases, and the Reynolds number based on the droplet diameter are sufficiently high. These requirements are easily fulfilled in this application. The key parameters involved in the fragmentation process are the aerodynamic forces, which tend to cause the breakup, and the surface tension forces, which act to hold the droplet together. Where the viscosity is high, this hinders deformation of the drop and acts to dissipate energy, thereby reducing the tendency to breakup. In general, this effect is not important where the Ohnesorge number

$$Oh = \frac{\mu_l}{\sqrt{\rho_l \sigma d_l}}$$

is less than 0.1 (5). The subscript l denotes liquid phase properties for viscosity μ, density ρ, diameter d and surface tension σ. This is easily true by some orders of magnitude for aluminium droplets smaller than 10mm in diameter, which results in the breakup being controlled exclusively by the Weber number

$$We = \frac{\rho_g V^2 d_l}{\sigma}$$

where the subscript g denotes the gas phase condition and V the relative velocity between the liquid and gas phases. There are a range of critical Weber numbers for different regimes of breakup, driven by the relative importance of the aerodynamic and surface tension forces. These are given in Table 3 taken from Jain (6).

Regime	We Range
Vibrational (no breakup)	$0 < We <\sim 11$
Bag breakup	$\sim 11 < We <\sim 35$
Multimode breakup	$\sim 35 < We <\sim 80$
Sheet thinning breakup	$\sim 80 < We <\sim 350$
Catastrophic breakup	$We >\sim 350$

Table 3: Critical Weber Numbers for Break-up Regimes (6)

The gradually increasing Weber number results in the regimes which are shown in Figure 30, which are reproduced from Jain et al. (7). Frame (a) shows bag breakup, where the droplet turns inside-out and shatters, producing a bimodal droplet distribution with small droplets from the bag and larger drops from the toroidal ring. Frames (b) and (c) show multimodal breakup, with a number of bags produced, and frame (d) shows sheet thinning (stripping) breakup where a sheet is formed at the edge of the droplet which evolves into ligaments and which then break up into multiple particles. A core droplet is sometimes left in the centre.

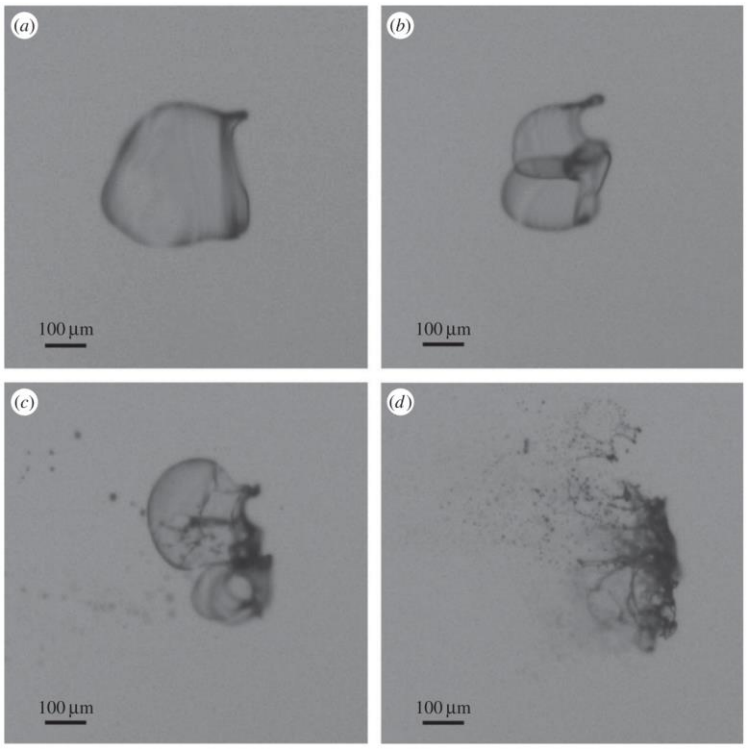

Figure 30: Secondary breakup at increasing Weber number (7)

Faeth (5) provides a simple correlation for the resultant Sauter Mean Diameter (d_{32}), which is defined for a droplet size distribution $n(d)$ where d is the droplet diameter as

$$d_{32} = \frac{\int n(d) d^3 \, dd}{\int n(d) d^2 \, dd}$$

This is a very useful parameter as it provides a direct link between the total surface area of the droplets, which is of key interest for environmental impact, and the mass of the droplets produced. The correlation is claimed to be independent of the breakup regime, and is

$$d_{32} = 0.09 d_0$$

where d_o is the original droplet diameter.

There is a range of surface tension measurements for aluminium, with pure aluminium being of the order of 1.1N/m, and oxidised aluminium being approximately 0.89N/m. The lower value is taken for this analysis, although it is counter-intuitive that the surface tension is reduced due to the presence of an oxide layer, particularly given the behaviour observed in tests. The liquid density of aluminium is taken as 2375kg/m^3 and the viscosity as 1.65e-3Pa.s, which is the upper limit.

As well as the droplet size distribution produced in the fragmentation process, the timescales for the fragmentation process are also of interest. In order that the heating of the fragmented droplets occurs prior to the droplet deceleration, the process has to be sufficiently fast. Figure 7 and Figure 8 in Section 2.3.1 suggest that timescales of the order of 0.1s-1s are required for droplets of 1mm or over to fragment such that the remaining velocity is sufficient that the heating of the produced droplets can be modelled sufficiently well using their resultant size.

The timescale for bag breakup is given by

$$t_b = \pi \sqrt{\left(\frac{\rho_l d^3}{16\sigma}\right)}$$

and that for stripping breakup by

$$t_s = C \frac{d}{2V} \sqrt{\frac{\rho_l}{\rho_g}}$$

where the constant C can be as high as 20.

Bag breakup timescales are a not a function of the air density, so for the purpose here, are simply a function of the droplet size. They are given in Table 4, and are sufficiently short that the breakup results can be considered in all cases.

Diameter (mm)	10	3	1	0.3	0.1	0.03
Timescale (s)	0.04	0.007	0.001	0.0002	0.00005	0.000007

Table 4: Bag Breakup Timescales

For stripping breakup, the timescales are density dependent, and so are shown in Figure 31 for the three largest particle sizes using $C = 1$. The timescales are sufficiently short at 100km, and would be even using $C = 20$, and so breakup can be assumed for all particles when the Weber number conditions are met.

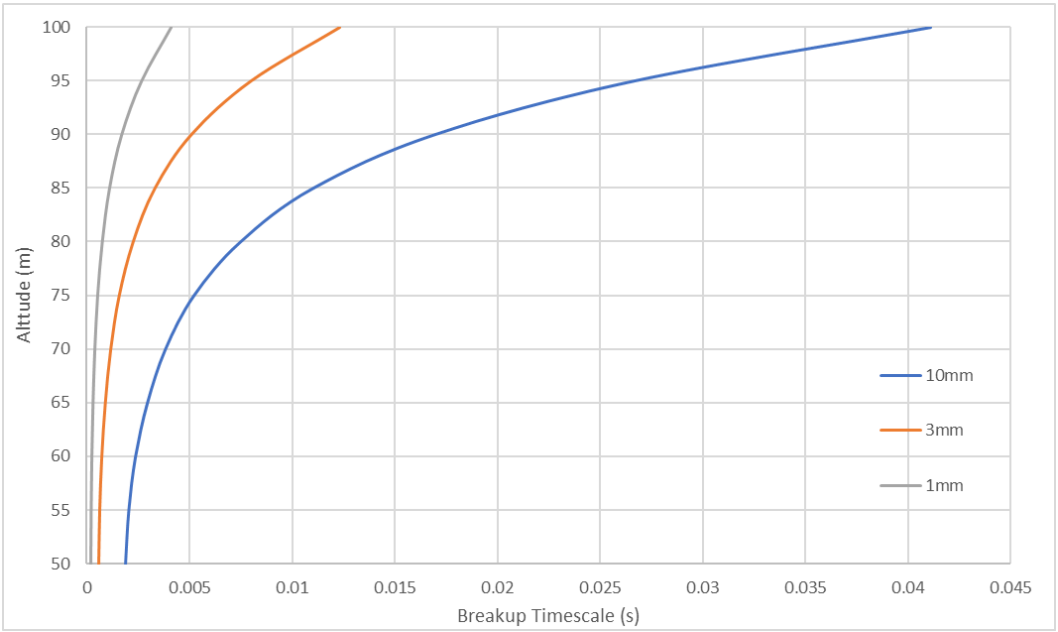

Figure 31: Stripping Breakup Timescales for Particles over 1mm Diameter

The Weber number can be calculated for each of the particle sizes as a function of altitude. This is done in Figure 32, and immediately demonstrates that the critical Weber number, $We = 11$, is not achieved by the particles under 1mm in size. This is significant as it does not drive the particle sizes to smaller values than have been already assessed in Section 2.3.

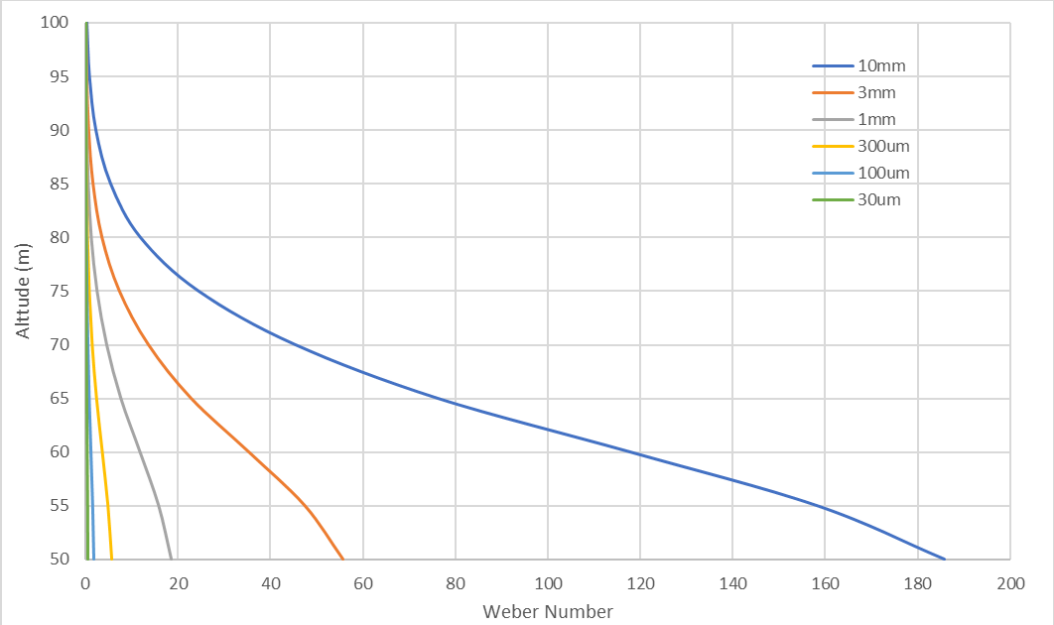

Figure 32: Weber Numbers for all Droplets and Altitudes

For the larger particles, 1mm particles reach the break-up criterion at 60km, 3mm particles at 70km and 10mm particles at 80km. The dominant breakup regime is bag breakup.

Given the Faeth correlation for the resultant particle sizes, it is proposed to simply reduce the particle size by an order of magnitude at fragmentation in order to capture the new mean diameter of the resultant particles in a surface area-to-mass ratio sense.

2.5 Mass Transfer Assessment

The assessment of the mass transfer of the particles follows the work of Vondrak et al. (8), which uses Langmuir evaporation. This assumes that the rate of evaporation into a vacuum is equal to the rate of evaporation needed to balance the rate of uptake of the species in a closed system. For a single species system, the rate of mass release is

$$\frac{dm}{dt} = \gamma p S \sqrt{\frac{\mu}{2\pi k_B T}}$$

where γ is the sticking coefficient, p is the thermodynamic equilibrium pressure of the species in the gas phase, S is the particle surface area, μ is the molecular weight and k_B is the Boltzmann constant. The sticking coefficient is zero below, and 1 above the melting point of multi-species meteoroids, which is taken as 1800K in (8). This is significantly below the aluminium oxide melt point, so it is not clear whether this temperature should be maintained in this analysis, or whether no mass transfer prior to melt should be allowed. In order to be conservative, mass transfer is allowed from 1800K.

The relative molecular mass of aluminium oxide (Al_2O_3) is 102, which leaves the remaining parameter as the thermodynamic equilibrium pressure. This is temperature dependent, and can be found for both aluminium and aluminium oxide in Lide (9). The values obtained are given in Table 5.

Pressure (Pa)	Vapour Temperature (K)	
	Aluminium	Aluminium Oxide
1	1482	
10	1632	
100	1817	2395
1000	2054	2623
10000	2364	2902
100000	2790	3248

Table 5: Vapor Pressures of Aluminium and Aluminium Oxide

Values at lower pressures for aluminium oxide have also been sought, with (10) giving a value of 0.133Pa at 1823K. Figure 33 is provided by Kim et al. (11), and is consistent with Table 5.

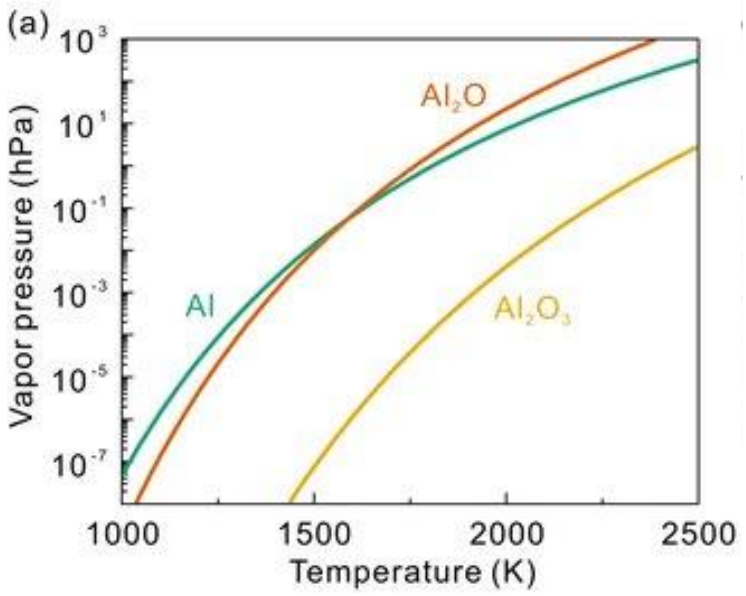

Figure 33: Aluminium and Aluminium Oxide Vapour Pressure (from (11))

Consolidating these data and adding a fit gives the curve shown in Figure 34. The fit is for the log (to base 10) of the vapour pressure as a function of the temperature.

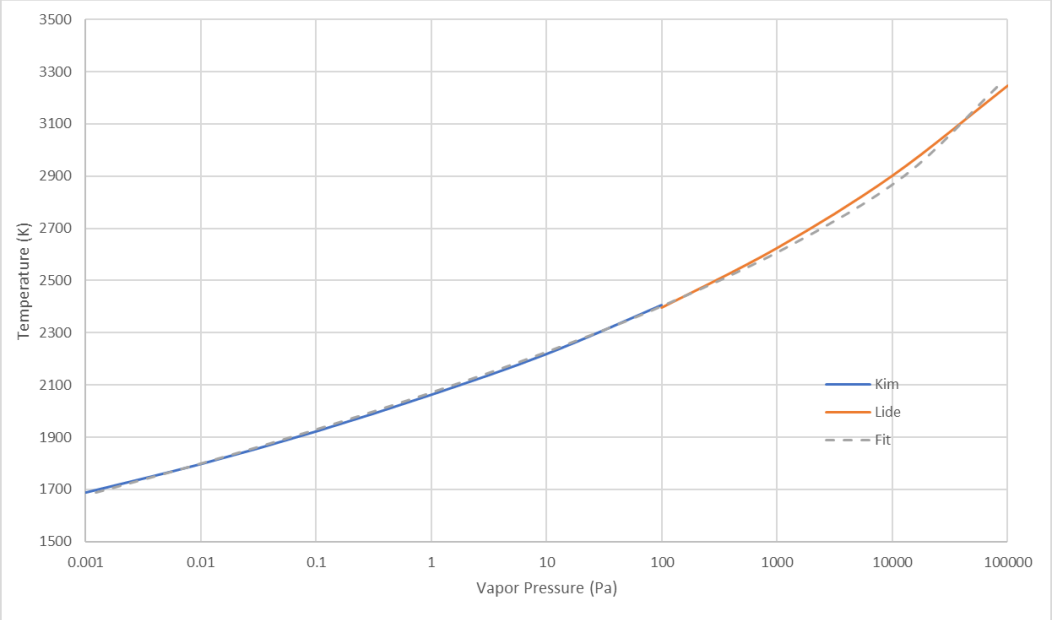

Figure 34: Fit Vapour Pressure Data for Aluminium Oxide

It is given by

$$\log(p) = -2.1889\left(\frac{T}{1000}\right)^2 + 15.823\frac{T}{1000} - 23.377$$

and can now be used with the outputs of Section 2.3 in order to provide the first estimate of the amount of material that is vaporised from different sizes of particle at different altitudes.

Using this model, a set of tables of the mass fraction vaporised can be constructed as a function of the particle diameter and the release altitude. These tables can be viewed as a vaporisation map showing which particles can produce vapour, and where that vapour can be produced.

2.5.1 Vaporisation Map (Aluminium Oxide Particle Surface Properties)

Using the temperature profiles generated in Section 2.3.2, the mass transfer equation is applied in order to provide an estimate of the mass of the particle which would be vaporised in each case. As this is a first order calculation, the geometry of the particle will be assumed constant, with the removed mass affecting neither the particle size, nor the drag/heating parameters. Given the large uncertainties involved, this provides a sensible first estimate of the mass transfer.

The mass transfer analysis has been performed in 5km steps, from 50km to 90km, for the six particle sizes, ranging from 30µm to 10mm. The temperatures which were reached using the pure aluminium oxide properties were relatively low, which suggested that the vaporisation would be limited, but was most likely to be observed in the 60-75km altitude range. The mass transfer results are in line with this, with the fraction of mass lost shown in Table 6 to Table 9. The scales have been designed to show cases with exactly no mass transfer in white, and then all cases with mass transfer on a colour scale from green to blue, even if the mass transfer is very small.

	10mm	3mm	1mm	300um	100um	30um
90km	0.000	0.000	0.000	0.000	0.000	0.000
85km	0.000	0.000	0.000	0.000	0.000	0.000
80km	0.000	0.000	0.000	0.000	0.000	0.000
75km	0.000	0.000	0.000	0.000	0.000	0.000
70km	0.000	0.000	0.000	0.000	0.001	0.004
65km	0.000	0.000	0.000	0.001	0.003	0.019
60km	0.000	0.000	0.000	0.000	0.001	0.019
55km	0.000	0.000	0.000	0.000	0.000	0.000
50km	0.000	0.000	0.000	0.000	0.000	0.000

Scale
1.0
0.9
0.8
0.7
0.6
0.5
0.4
0.3
0.2
0.1
0.0

Table 6: Mass Fraction of Particles Vaporised on Shallow Trajectory, Standard Ballistic Coefficient

	10mm	3mm	1mm	300um	100um	30um
90km	0.000	0.000	0.000	0.000	0.000	0.000
85km	0.000	0.000	0.000	0.000	0.000	0.000
80km	0.000	0.000	0.000	0.000	0.000	0.000
75km	0.000	0.000	0.000	0.000	0.000	0.001
70km	0.000	0.000	0.000	0.002	0.006	0.022
65km	0.000	0.000	0.000	0.006	0.033	0.138
60km	0.000	0.000	0.000	0.007	0.056	0.412
55km	0.000	0.000	0.000	0.000	0.016	0.123
50km	0.000	0.000	0.000	0.000	0.001	0.011

Scale
1.0
0.9
0.8
0.7
0.6
0.5
0.4
0.3
0.2
0.1
0.0

Table 7: Mass Fraction of Particles Vaporised on Shallow Trajectory, High Ballistic Coefficient

	10mm	3mm	1mm	300um	100um	30um
90km	0.000	0.000	0.000	0.000	0.000	0.000
85km	0.000	0.000	0.000	0.000	0.000	0.000
80km	0.000	0.000	0.000	0.000	0.000	0.000
75km	0.000	0.000	0.000	0.000	0.001	0.002
70km	0.000	0.000	0.000	0.002	0.008	0.028
65km	0.000	0.000	0.000	0.004	0.022	0.093
60km	0.000	0.000	0.000	0.001	0.010	0.081
55km	0.000	0.000	0.000	0.000	0.000	0.002
50km	0.000	0.000	0.000	0.000	0.000	0.000

Scale
1.0
0.9
0.8
0.7
0.6
0.5
0.4
0.3
0.2
0.1
0.0

Table 8: Mass Fraction of Particles Vaporised on Steep Trajectory, Standard Ballistic Coefficient

	10mm	3mm	1mm	300um	100um	30um
90km	0.000	0.000	0.000	0.000	0.000	0.000
85km	0.000	0.000	0.000	0.000	0.000	0.000
80km	0.000	0.000	0.000	0.000	0.000	0.000
75km	0.000	0.000	0.000	0.000	0.001	0.002
70km	0.000	0.000	0.000	0.003	0.021	0.056
65km	0.000	0.000	0.000	0.032	0.155	0.609
60km	0.000	0.000	0.000	0.049	0.316	1.000
55km	0.000	0.000	0.000	0.001	0.093	0.649
50km	0.000	0.000	0.000	0.000	0.004	0.060

Scale
1.0
0.9
0.8
0.7
0.6
0.5
0.4
0.3
0.2
0.1
0.0

Table 9: Mass Fraction of Particles Vaporised on Steep Trajectory, High Ballistic Coefficient

The tables are consistent in showing that the particles of 1mm and over do not reach sufficient temperature to vaporise, with the exception of 1mm particles at 60km on the most energetic trajectory. The standard ballistic coefficient cases show under 10% vaporisation, and no vaporisation at 80km and above, or 50km and below. More vaporisation is suggested on the higher ballistic coefficient trajectories, although only the steep trajectory shows more than 10% of a 100µm particle vaporising at any altitudes (60-65km), with more than 50% of a 30µm particle vaporising between 55km and 65km.

Overall, this suggests a low vaporisation of aluminium oxide for particle sizes of interest released from spacecraft in demise, assuming that the processes observed in wind tunnels are relevant. Importantly, this assumes that the heat transfer to the particles is limited by the catalycity of the oxide surface, which results in lower temperatures and less vaporisation.

2.5.2 Vaporisation Map (Aluminium Test Particle Surface Properties)

Moving to the case where the particle surface properties reflect those for oxidised aluminium surfaces in wind tunnel demise tests, which is likely to be the case for large particles, but is less justifiable for small particles, the results are different. Here, the continuum heat transfer includes the energy from catalytic recombination of oxygen atoms, and thus the temperatures reached are significantly higher.

Once again, the four different trajectories are assessed, and the vaporisation observed is increased. The results are shown in Table 10 to Table 13. The relative behaviour of the different trajectories is similar to the previous case, with the higher ballistic coefficient maintaining a higher velocity lower into the atmosphere, resulting in higher heating, and thus vaporisation.

	10mm	3mm	1mm	300um	100um	30um
90km	0.000	0.000	0.000	0.000	0.000	0.000
85km	0.000	0.000	0.000	0.000	0.001	0.001
80km	0.000	0.000	0.000	0.024	0.062	0.112
75km	0.000	0.000	0.003	0.728	1.000	1.000
70km	0.000	0.000	0.000	1.000	1.000	1.000
65km	0.000	0.000	0.000	1.000	1.000	1.000
60km	0.000	0.000	0.000	1.000	1.000	1.000
55km	0.000	0.000	0.000	0.000	0.562	1.000
50km	0.000	0.000	0.000	0.000	0.002	0.033

Scale
1.0
0.9
0.8
0.7
0.6
0.5
0.4
0.3
0.2
0.1
0.0

Table 10: Mass Fraction of Particles Vaporised on Shallow Trajectory, Standard Ball. Coeff.

	10mm	3mm	1mm	300um	100um	30um
90km	0.000	0.000	0.000	0.000	0.000	0.000
85km	0.000	0.000	0.000	0.000	0.001	0.002
80km	0.000	0.000	0.000	0.003	0.103	0.168
75km	0.000	0.000	0.000	0.912	1.000	1.000
70km	0.000	0.000	0.004	1.000	1.000	1.000
65km	0.000	0.000	0.001	1.000	1.000	1.000
60km	0.000	0.000	0.014	1.000	1.000	1.000
55km	0.000	0.000	0.000	1.000	1.000	1.000
50km	0.000	0.000	0.000	0.114	1.000	1.000

Scale
1.0
0.9
0.8
0.7
0.6
0.5
0.4
0.3
0.2
0.1
0.0

Table 11: Mass Fraction of Particles Vaporised on Shallow Trajectory, High Ballistic Coefficient

	10mm	3mm	1mm	300um	100um	30um
90km	0.000	0.000	0.000	0.000	0.000	0.000
85km	0.000	0.000	0.000	0.000	0.002	0.002
80km	0.000	0.000	0.000	0.006	0.159	0.257
75km	0.000	0.000	0.000	1.000	1.000	1.000
70km	0.000	0.000	0.000	1.000	1.000	1.000
65km	0.000	0.000	0.000	1.000	1.000	1.000
60km	0.000	0.000	0.000	0.123	1.000	1.000
55km	0.000	0.000	0.000	0.006	1.000	1.000
50km	0.000	0.000	0.000	0.000	0.007	0.108

Scale
1.0
0.9
0.8
0.7
0.6
0.5
0.4
0.3
0.2
0.1
0.0

Table 12: Mass Fraction of Particles Vaporised on Steep Trajectory, Standard Ballistic Coefficient

	10mm	3mm	1mm	300um	100um	30um
90km	0.000	0.000	0.000	0.000	0.000	0.000
85km	0.000	0.000	0.000	0.000	0.002	0.003
80km	0.000	0.000	0.000	0.094	0.215	0.387
75km	0.000	0.000	0.000	1.000	1.000	1.000
70km	0.000	0.000	0.034	1.000	1.000	1.000
65km	0.000	0.000	0.014	1.000	1.000	1.000
60km	0.000	0.000	0.000	1.000	1.000	1.000
55km	0.000	0.000	0.000	1.000	1.000	1.000
50km	0.000	0.000	0.000	0.770	1.000	1.000

Scale
1.0
0.9
0.8
0.7
0.6
0.5
0.4
0.3
0.2
0.1
0.0

Table 13: Mass Fraction of Particles Vaporised on Steep Trajectory, High Ballistic Coefficient

With these surface property assumptions, particles of 300µm and smaller are fully vaporised, and particles of 1mm and larger remain in the solid phase. As 3mm particles are expected to break up from 70km, resulting in Sauter Mean diameters of 300µm particles, and 1mm particles are expected to breakup from 60km, this suggests that the vast majority of particles will vaporise when release below 60km, with a reasonable mass of the particle population vaporising below 70km.

This highlights that the determination of the surface properties of the particles is critical in the assessment of the atmospheric impact, with the difference in the predictions between the two cases ranging from almost no vaporisation, to highly significant vaporisation. Improved understanding of

particle surface properties is critical to the assessment of the atmospheric impact of aluminium demise.

2.6 Preliminary Release Altitude Assessment

In order to use these maps to predict the mass of vaporised aluminium oxide produced in a re-entry, some indication of the altitudes in which the aluminium is released is required. A first assessment of this was performed within the ATISPADE activity (3), based on results from a range of spacecraft simulated using the ESA SCARAB tool. Some care is required here, as the version of SCARAB used in this analysis is now known to underheat large compound objects, which means that the altitudes of demise are expected to be lower than would be predicted by tools with an improved representation of length scale. However, as the lower altitudes have been shown to be the most relevant for vaporisation, these results can be considered to provide a 'worst case' in terms of the altitude distribution of particle release.

The altitude distribution for shallow (uncontrolled) re-entries is shown in Figure 35, and shows a peak at 75km. The cumulative mass released is shown in Table 14, although it is worth re-iterating that this is understood to predict lower altitudes than would be the case with more recent best-practice analysis.

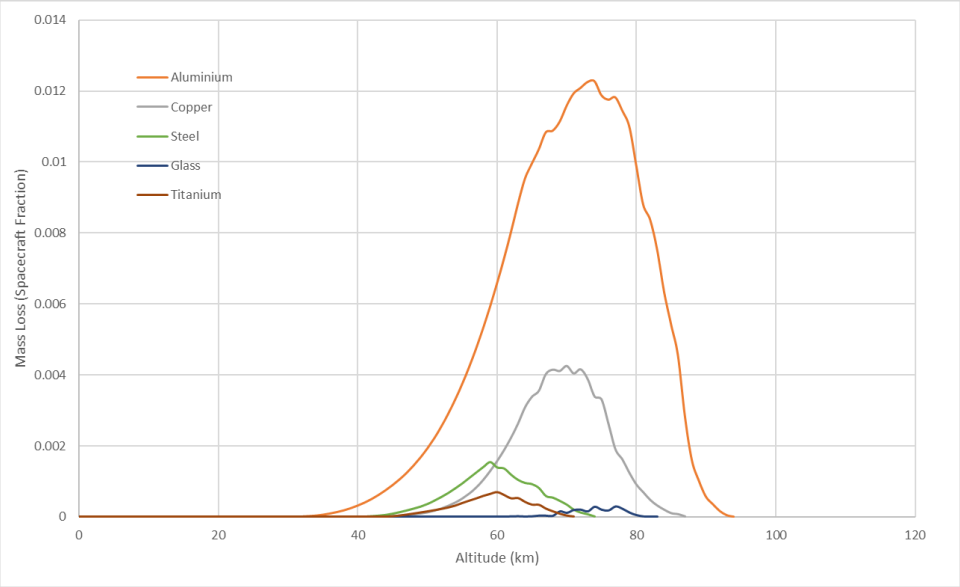

Figure 35: Altitude of Demise on Shallow Re-entry (from (3))

Altitude (km)	Aluminium Mass Release Fraction
90	<1%
85	4%
80	15%
75	34%
70	52%
65	70%
60	83%
55	92%
50	97%

Table 14: Cumulative Mass Release with Altitude (Shallow Trajectory)

Allied to the results using the aluminium surface properties, this would suggest that approximately half of the demised mass could potentially be vaporised in a standard uncontrolled re-entry, occurring between 75km and 60km, were all the particles to be smaller than 300µm in size.

A similar analysis on a steep (controlled) re-entry is based on the ATISPADE cumulative mass release shown in Figure 36, and the accompanying Table 15. Once again, it should be noted that the altitudes of release are likely to be low relative to more modern best-practice analyses.

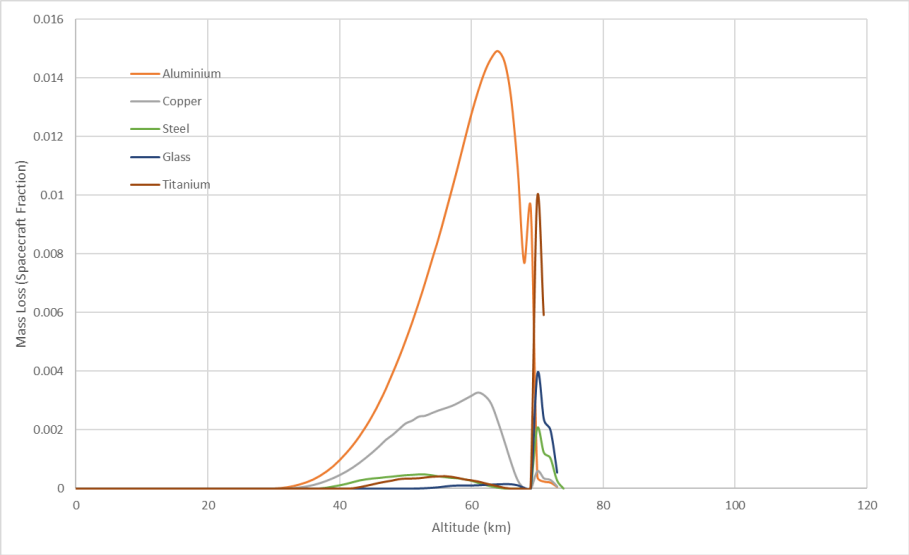

Figure 36: Altitude of Demise on Steep Re-entry (from (3))

Altitude (km)	Aluminium Mass Release Fraction
90	0%
85	0%
80	0%
75	0%
70	<1%
65	18%
60	48%
55	61%
50	87%

Table 15: Cumulative Mass Release with Altitude (Steep Trajectory)

Again, assuming the aluminium particle properties, and a 300µm size limit, this would suggest that the vast majority of demised aluminium will vaporise. This supports the previous assertions that controlled re-entries may have a higher impact on the atmosphere due to the demise occurring at lower altitudes.

2.7 Conclusions and Further Work

The analysis performed on the potential vaporisation of aluminium oxide, or oxide-coated aluminium particles, suggests that it is possible that a significant fraction of the aluminium mass from spacecraft could be vaporised, and thus deposited in the atmosphere as nanometre sized aluminium oxide particles. However, this work also shows that this is highly dependent upon a number of assumptions, not least the particulate surface properties, and that the effect could, potentially, be relatively small.

The critical aspect demonstrated in this work is the dependence on the catalycity of the particle surface. A low catalycity ceramic (aluminium oxide) surface would heat significantly less than a high catalycity surface as is observed for aluminium objects (with oxide layer) in wind tunnels. An improved understanding of the heat fluxes which are received by aluminium particles is critical to the understanding of the vaporisation potential.

It is also worth noting that this analysis has assumed that the vaporisation behaviour of aluminium oxide is dominant as this forms the outer layer of the particle. It is feasible that there is some aluminium metal vaporisation. This would serve to increase the material vaporisation as the vaporisation temperatures are lower for the unoxidized material.

The size distribution of produced particles is also a critical aspect of the analysis. It is known that relatively large particles are produced, but there is a possibility that these will break-up due to the high speed flow. It is not clear how many of the particles escape the wake of the demising object, and the analysis here assumes that all the particles reach the free stream flow.

A number of these aspects can potentially be tested in a high enthalpy wind tunnel test campaign. This can analyse the sizes of produced particles, the downstream break-up of particles, and the vapour produced, whether aluminium gas or aluminium oxide gas.

Although this analysis provides a useful first step in understanding the potential for aluminium vapour production, the uncertainties are very high. Consolidation of this analysis through ground testing is the next step.

3 CONSTRUCTION OF PLASMA WIND TUNNEL TEST PLAN

The study on the potential for vaporisation of aluminium from re-entering spacecraft has suggested a number of items which are required to be verified by test. Broadly, this can be split into two main themes. The first of these is a verification of the break-up of the particles/droplets. This is important as the vaporisation from smaller particles is much greater than from larger ones, and the study above suggests that particles of 3mm will break-up below 70km, and 1mm below 60km. As this is the altitude range where the vaporisation potential is highest, this can make a significant difference to the mass of nanoparticles produced.

The second aspect is a verification of the production of gaseous species from the particles produced. The analysis performed here has worked on the output from the ATV-1 observation campaign which suggests that aluminium oxide (AlO) is the primary gaseous species produced. However, there is a possibility that, particularly at higher altitudes, aluminium gas could be produced in higher quantities, and this could imply that there is a higher level of vaporisation. This needs to be verified. Further, the analysis has demonstrated that there is a high uncertainty in the heating to the particles, and that this is driven primarily (in the models, at least) from the surface property assumptions. Observing the gaseous production of aluminium species will require differences in diagnostic set-up to previous wind tunnel test campaigns.

For both aspects, there is a significant challenge in determining suitable conditions for the test. In both cases, there is a significant dependence of the theoretical results on the balance between the velocity of the particles and the ambient density. As the wind tunnel velocity will be below that observed in flight, some care must be used in the determination of the ambient density in order to obtain relevant conditions representative of desired altitudes. As the physical processes of interest are different in break-up and vaporisation, it is likely that different conditions will be required in each case.

3.1 Testing Objectives

With two distinct aspects to test, the test plan is split up into two campaigns, one for assessment of the likely sizes of particles produced, and one for the assessment of gaseous products.

3.1.1 Particle Size Assessment

The objectives of particle size assessment tests are:

- To assess the size of aluminium oxide fragments/particles ejected from demising spacecraft components.
- To verify the rapid break-up of molten aluminium particles/droplets of sufficient size.
- To assess the particle/droplet size distribution produced.
- To assess the variation of these effects at different pressures in order to capture the impact of altitude.

The size of the aluminium fragment produced during the demise process can be sufficiently large that it would still be reasonable to describe it as a fragment, rather than a particle. Molten aluminium fragments as large as a few centimetres across have been observed in testing (see Figure 4), and the peeling of millimetres thick sheets of aluminium have been seen from different component housings (see Figure 2). Therefore, there are a range of fragment/particle types which are relevant for study in this test campaign. These include:

- Molten droplets of aluminium from 100µm to 20mm in diameter.
- Molten sheets of aluminium of 1mm to 2mm thickness and 5cm side.
- Ligaments of aluminium of 10mm to 20mm length and 1mm diameter.

It is clear that the production of such objects in a molten form is a significant challenge. Droplets can be pre-melted and released from a crucible. The production of sheets and ligaments is likely to require a test sample, to be placed into the plasma wind tunnel, which produces the desired structures on melt. This is challenging, and will need to draw on experience from previous test campaigns. Clearly, the identification of the produced particles will need to be analysed closely, and high speed camera imagery is likely to be necessary to capture this. The intention here is to demonstrate the range of particle shapes and sizes which can be produced from typical aluminium spacecraft structures during the demise process.

For each of these produced particle types, an assessment is required of the break-up process. This can be performed in a plasma wind tunnel, but will need adaptation of the normal set-up. Some care is required here to match the Weber numbers in flight as the velocity of the particles in the wind tunnel will be lower than experienced in re-entry. The key issue here is that the majority of diagnostics are designed to be made *ahead* of the test sample, but the interest in this campaign is downstream of the test sample, in the particles which are being entrained into the flow. Furthermore, the diagnostics of the vaporised species are usually captured in the boundary layer of the test sample, where in this case, the interest is in the vapour produced downstream of the sample. Again, support from a high speed camera would be helpful in determining trajectories of particles in order to relate them to the vapour produced.

A critical question is whether the test sample required to produce the particles can be designed in such a way as to minimise the blockage of the flow, reducing effects of the wake of the sample on the particle behaviour. It is possible that this can have an impact on the effective Weber number encountered by the particle, and thus the break-up process.

From the break-up measurements, the intended outputs are understanding of the conditions under which the different types of particle/droplet break-up, and the resultant particle size distribution. These form important inputs for the vaporisation assessment part of the activity. Determination of the particle size distribution is non-trivial, and it may not be possible to do this well within a plasma wind tunnel. Droplet size measurement apparatus for metal sprays exist, and there are academic test facilities which perform these measurements for thermal spray applications. Some assessment is required as to whether these instruments could be used in conjunction with a plasma wind tunnel.

The final requirement concerns the conditions for test. Matching the test conditions to be relevant to different altitudes in re-entry is non-trivial, and it is clear that a number of different ambient density conditions are required in order to match the range of density conditions which are experienced in flight. Given the results of the first part of this work, the 50km-85km range is targeted.

3.1.2 Particle Vaporisation Assessment

The objectives of the particle vaporisation assessment are:

- To assess the amount of vapour produced for a range of particle sizes at a range of ambient pressures.
- To determine the major gaseous species produced for different particle sizes and conditions.
- To attempt inference of the relevant particle surface properties for use in vaporisation assessment calculations.

The expectation here is that there will be significant breakup of the aluminium sheets and ligaments, resulting in smaller particles, which are reasonably approximated by a sphere. This may not be the case, and larger remaining particles will certainly act to reduce the vaporisation rate and limit the impact of re-entering spacecraft aluminium on the atmosphere.

The intention is to perform these tests with approximately a monodisperse particle size distribution, releasing the particles into the flowfield. In this setup, it is intended that there will be no sample blocking the flow, and that the particles will remain in the freestream jet, being entrained as they would during re-entry. It is possible that some break-up may be observed for larger droplets at larger flow densities, which could consolidate data from the break-up campaign.

The particle vaporisation is intended to be measured using optical emission spectroscopy, with both aluminium and aluminium oxide being detectable in the ultra-violet spectrum (see Figure 1). The vaporisation will be downstream of the particle introduction into the flow, and is required to be measured along the path of the particle in order to detect any vaporisation. The location of the vapour detection is important as it correlates to the heating rate of the particle, and determining the heating rate of the particle allows inference of the surface properties.

It is possible that in cases where the gas density is low, the particles may not reach sufficient temperature to vaporise before they are swept into the diffuser. In this case, it may be necessary to heat the particles to higher temperature before releasing them into the flow.

3.2 Test Campaigns

This section will outline the test methodology for each campaign, and describe the instrumentation which can be used to capture the necessary data. It will also provide a first iteration of the analysis deriving the test flow conditions.

3.2.1 Break-up Assessment

A standard plasma wind tunnel set-up is shown in Figure 37. This demonstrates that the observation windows are designed to be upstream of the sample, such that they can focus on the sample surface.

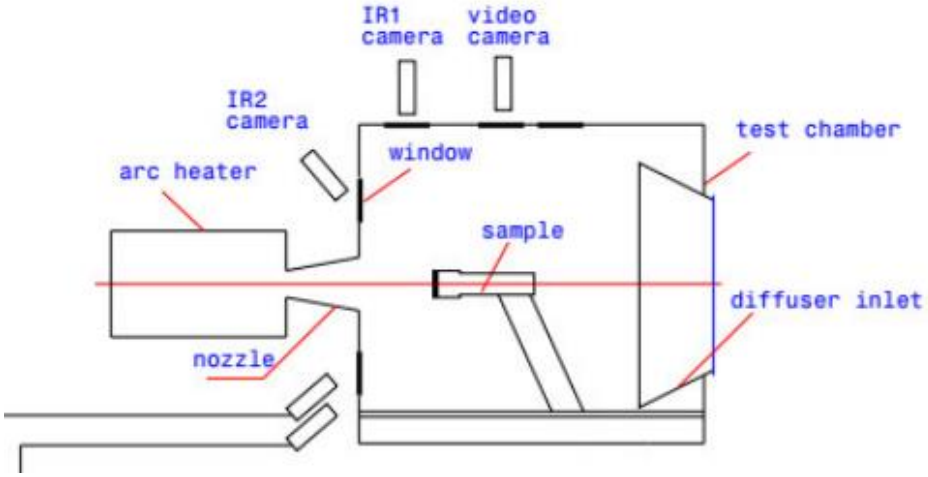

Figure 37: Standard Plasma Wind Tunnel Set-up

For the purpose of understanding the products of demise, the instrument focus is required to be downstream of the test sample, which can cause significant difficulty as the observation windows are often not situated in suitable locations. For the break-up assessment, a test sample is still required for the ligaments and sheets analysis, as a method to generate these shapes of molten aluminium is required. For this, it is suggested to place the sample as close to the nozzle exit as is practical, and to construct a sample which is held from the sides in order to avoid blockage of the nozzle plume. This has been done in previous activities and is not expected to be an issue. The limit for the sample placement is often driven by the optical access such that the sample can be observed.

This allows the majority of the test section to be dedicated to the observation of the particle break-up. For this part of the activity, HD video cameras and high-speed cameras are the most useful diagnostics. There are also laser diagnostics which can be used to infer the velocity of particles between two points, and for small particles, the entrainment into the freestream can be used as a diagnostic of the particle size. The most appropriate for use in this case is Particle Image Velocimetry (PIV) which is normally used to determine the velocity of the flowfield from a set of small tracer particles which are seeded into the flow. In this case, the idea is to use the principles of the technique to measure the velocity of particles which are produced by the demise of the test object. This allows the entrainment of the particles into the flow to be determined, which allows the drag of the particles, and thus their size to be assessed.

This is also expected to be a useful tool for observing particle break-up as illuminated images of the particles in the flowfield will be obtained. As this provides visual data, it can be used as a basic visual camera diagnostic as well. This is appropriate for all the input particle types and sizes.

There are also other fields of work in which the fragmentation of molten metallic particles are of interest. Thermal spraying techniques are coating processes in which molten metal sprays are used to coat ferrous materials in order to protect against corrosion. A wire form of the metal is melted by an energy source and sprayed onto another metal surface. Aluminium is a commonly used metal for this process. Researchers such as Lunn et al. (12) have performed experiments to assess the break-up of aluminium droplets released from a 2.3mm diameter wire in the process. The high pressures used result in the Weber numbers being significantly above those which will be observed in re-entry, as the air flow is pressurised, and they see particles with a number mean of 70µm. The mass mean will be a little higher, probably around 100µm. Detection of the particle motion was performed using a laser strobe technique. However, it should be noted that the camera frame rate was not sufficiently fast to capture the break-up event, and a large number of events were required in order to obtain representative data. Given the small number of tests which can be performed in a plasma wind tunnel, this suggests that some care is required in ensuring that suitable diagnostics can be produced.

Given the similarity between a laser strobe set-up and a PIV system, this type of optical diagnostic appears to be the most suitable approach for obtaining the necessary data on the particle sizes post-break-up, and the conditions under which break-up occurs. In order to produce sufficient data, it is suggested that a significant number of objects/particles are demised in a single test. This can be done for molten droplets, but is significantly more challenging for ligaments, and may not be possible for sheets due to the required heat-up time and surface area of the sheets. This could limit the effectiveness of the sheet testing.

3.2.1.1 Test Samples

Three types of test sample are considered; sheets, ligaments and droplets. For all three sample types, it is preferable to construct a test where a large number of samples can be tested within a single run of the facility. This both increases the data gained per test, but also mitigates against the need for very high-speed optics as the probability of obtaining good data increases with the number of particles which can be analysed within the test.

The most straightforward particle dispensing method is the use of a crucible in order to produce approximately spherical droplets. A set of crucibles producing different sizes of droplets will be required in order to test the range of suitable droplet sizes. These crucibles will require heating such that the aluminium contained within them melts, and it may be required to provide some pressure such that the liquid aluminium is dripped from the crucible into the flow. It is possible that gravity will be sufficient, but, particularly as the droplet size decreases, it will be important to ensure that the aluminium will be released from the crucible. It is expected that, for the relatively small droplets being produced, that the rate of droplet production will not be too fast. Within the COPPER activity (13), a boron nitride crucible was used to release aluminium droplets, although the droplets were larger in this case. An induction coil was used to heat the crucible, as shown in Figure 38. A range of crucibles will be required in order to be able to produce droplets from 100µm to 20mm in size.

Figure 38: Boron Nitride Crucible with Induction Coil

In order to seed a number of ligaments into the flow, a sample which resembles a comb is foreseen. A set of aluminium teeth, of the required 1mm diameter and 10mm or 20mm length will be attached to a steel bar of square cross section. The attachment will be a push fit into holes of 1.2mm diameter. In order that the aluminium melts, a high-temperature ceramic glue is suggested for use to hold the ligaments into the steel bar. Depending on the size of the test facility, a bar of 20-50cm length is foreseen, which would allow some tens of aluminium ligaments to be tested, depending on the required spacing between the ligaments. It is expected that it will not be necessary to use a spacing greater than 2mm. A steel pet comb is shown in Figure 39, which demonstrates the basic design concept. The steel bar will be considerably thicker for this application in order to ensure that there is a sufficient heat sink that only the aluminium ligaments are melted.

Figure 39: Ligament 'Comb' Test Concept

The idea of the test is that the thin aluminium parts will heat and melt whilst the steel bar remains intact. In order to obtain a stream of molten aluminium ligaments, it is envisaged that the whole assembly is held above the flow, and is gradually lowered, with a sufficiently slow speed that the aluminium is melted at the top of the flow, such that gravity acts to take the material into the flow core, rather than causing it to fall out of the bottom of the core.

Designing a suitable sample for the testing of a number of sheets is a greater challenge. In this case, the time taken to bring a sheet up to the melting point of aluminium is significantly larger, and so the sheets cannot be individually heated. The most appropriate concept is to use an approach similar to the comb, but with thin 'blades' of aluminium, attached to a central steel rod. In this case, a high-temperature ceramic adhesive connection will be more important, as the 'blades' are required to tear from the rod as this is representative of the phenomena seen in equipment demise tests. It is expected that it will be possible to mount a sheet at least every 20 degrees. The concept is similar to a Savonius wind turbine, shown in Figure 40, but with a larger number of straight blades, and a central spine. The concept is shown schematically in Figure 41.

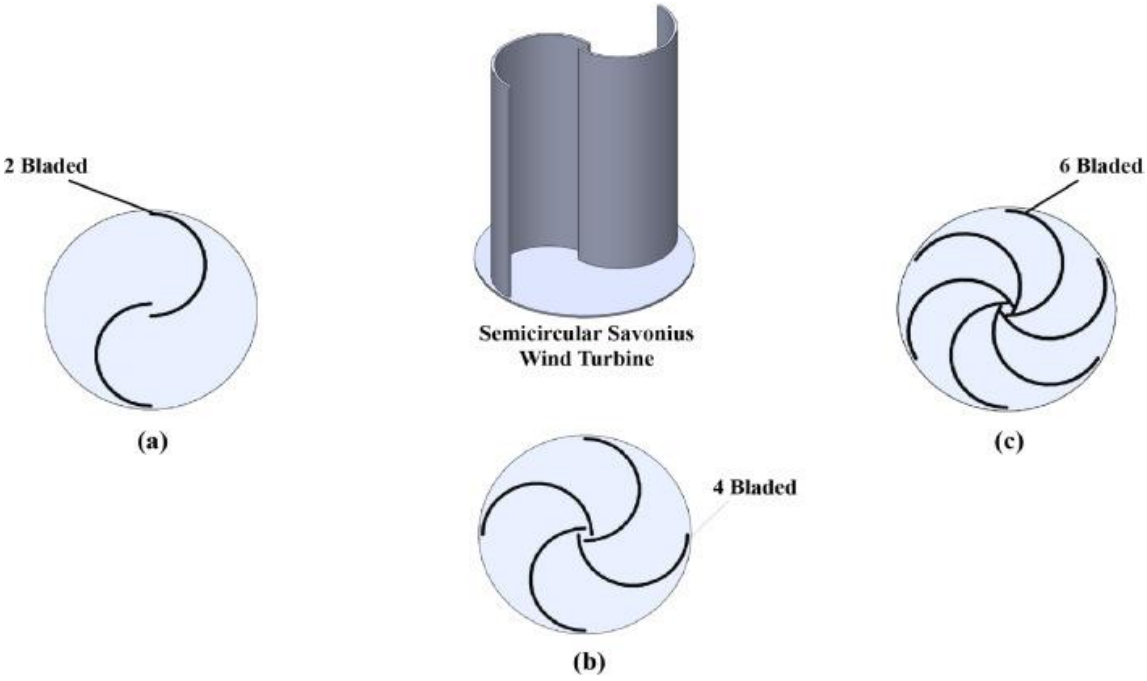

Figure 40: Savonius Wind Turbine

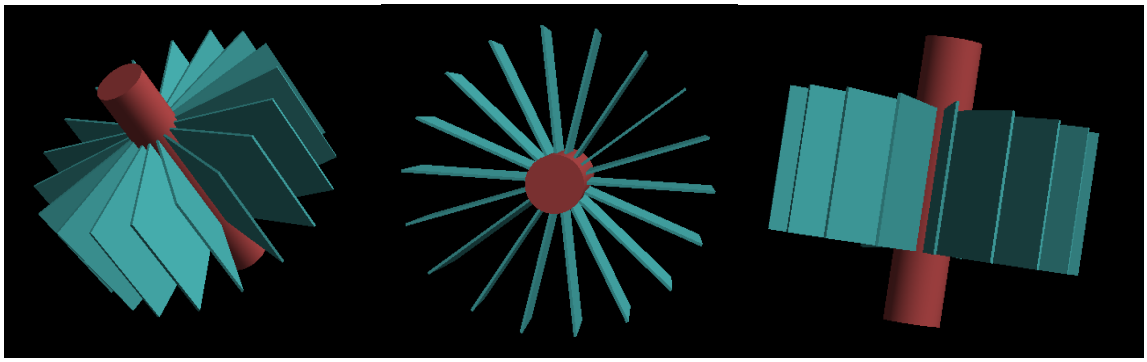

Figure 41: Central Rod with Aluminium 'Blades' (3 Views)

This carousel of aluminium sheets is designed to be rotated, such that each of the blades becomes exposed to the flow, and the failure of the sheets occur at similar times such that good optical data can be obtained. The rotation rates required are slow, it is expected that 0.25Hz would be sufficient.

There is already a rotation device existent within the DLR L2K wind tunnel, which is shown in Figure 42. This device would be ideal, but it should be noted that the test setup proposed here, with the relatively slow rotation rates does not require such a robust installation.

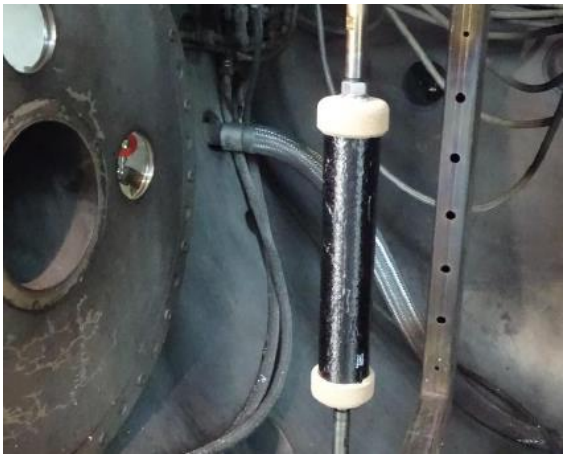

Figure 42: DLR Rotation Device

3.2.1.2 Test Set-up

The overall experimental set-up is thus as shown in Figure 43. The sample shown is a crucible delivering molten aluminium particles, but the set-up is consistent for the ligament and sheet samples. This is set-up as close to the nozzle as is practical, leaving as much of the test section as possible for assessment of the particle break-up. There is one HD camera focussed on the particle delivery, and fragmentation of the ligaments and sheets, and another looking along the flow, intending to capture a view of the particles (post, or possibly during, fragmentation) in flight. A high speed camera is focussed along the line of the flow in order to observe break-up events once the samples have been entrained into the air flow. The PIV setup is shown as a broad box as the idea here is to capture the velocities of the particles over a large distance in order to capture as much data as possible, and to increase the likelihood of observing fragmentation events.

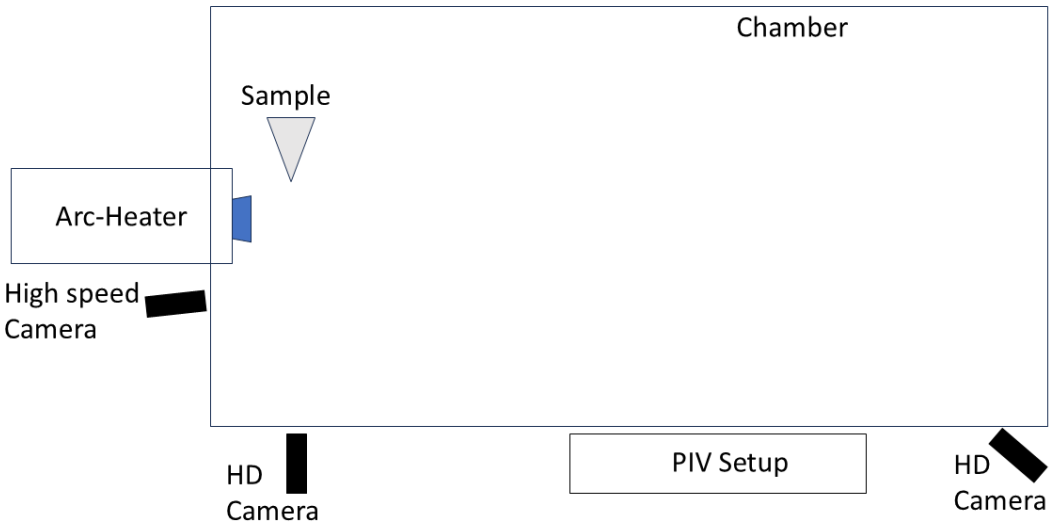

Figure 43: Basic Break-up Test Set-up

3.2.1.3 Test Conditions Derivation

Setting the test conditions for the campaigns is a non-trivial task, in part due to the need to keep the analysis general, as a specific wind tunnel has not been identified. The test conditions for most plasma wind tunnel facilities are defined mainly in terms of heat flux and dynamic pressure. For the break-up

analysis, the important quantity is the Weber number, which is defined as

$$We = \frac{\rho_g V^2 d_l}{\sigma}$$

with ρ_g being the (flow, not ambient) gas density, V the velocity, d_l the particle diameter and σ the surface tension. The dependence on d_l implies that the Weber number will vary for different particle sizes, and so suitable Weber numbers need to be chosen such that the threshold size for particle break-up can be assessed.

In most plasma wind tunnels, the flow will be such that the melt temperature of aluminium will be exceeded at all achievable conditions for the test samples which are planned for use. This makes the selection of the heat flux condition less critical, but a heat flux condition at the lower end is preferred as this enhances the survivability of the steel sample holders, allowing their use in multiple tests, and potentially multiple test campaigns.

As dynamic pressure is defined by

$$q = \frac{1}{2}\rho V^2$$

this is related to the Weber number via

$$We = \frac{2qd}{\sigma}$$

Using 0.89N/m for the molten aluminium surface tension, the dependence of the Weber number on the dynamic pressure and particle density can be obtained. For reference, the dynamic pressures on the standard trajectories used for the analysis in Section 2.1 are shown in Figure 44. The dynamic pressures of interest range between about 250Pa (80km) and go as high as 10000Pa (55km).

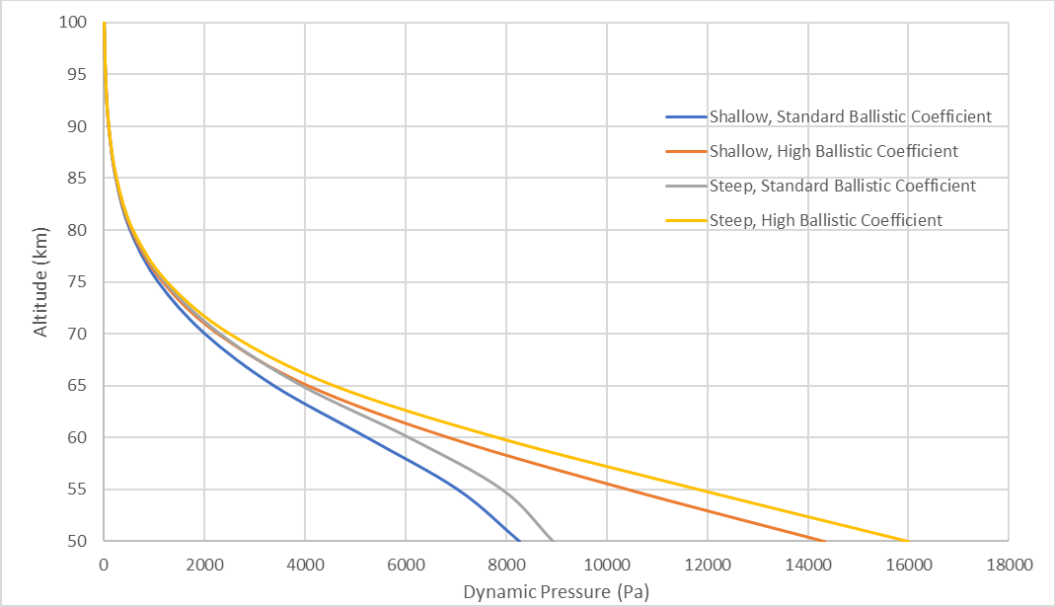

Figure 44: Dynamic Pressure on Reference Trajectories

Different plasma wind tunnels will be able to produce different dynamic pressures. The L2K facility at DLR is capable of covering 250Pa to at least 4000Pa, which covers the 80km to 65km range for the standard ballistic coefficient re-entries. Importantly, this results in the Weber number reaching the

threshold value of 11 for particles over 2mm in diameter, as shown in Figure 45, which would be expected to result in break-up of both ligaments and sheets. For the testing of individual particles, it is recommended to start with the larger particles, and reduce the size in tests to the point where no break-up is observed. This is likely to be once the particle diameter reaches 1mm, but this is not guaranteed.

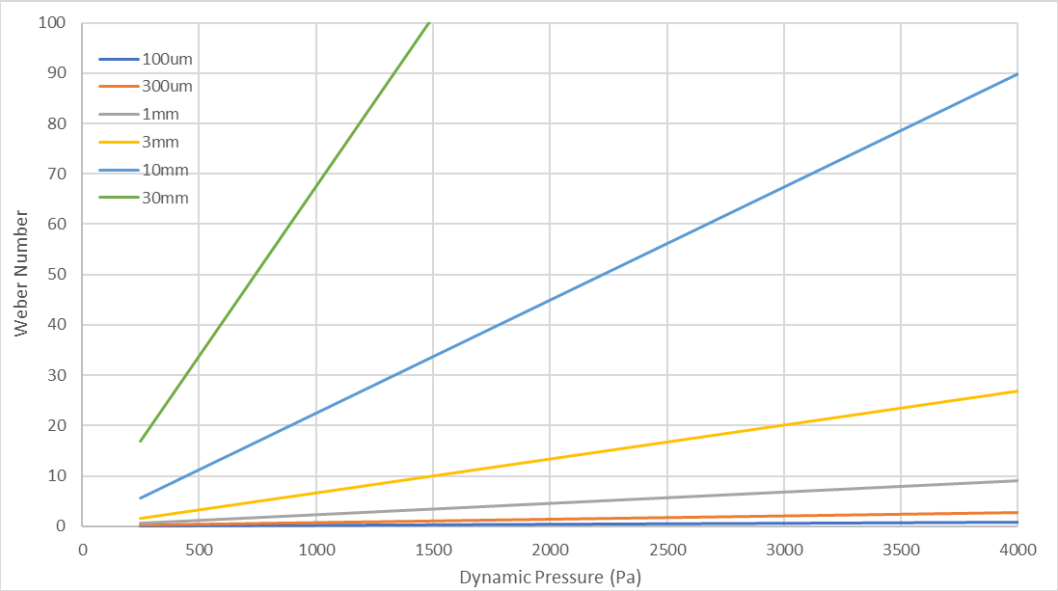

Figure 45: Weber Numbers

3.2.1.4 Preliminary Test Matrix

A preliminary test matrix has been constructed assuming that twelve tests can be performed in the wind tunnel. Given the restriction of the number of tests, there is a possible benefit of running multiple crucibles in a single test, allowing more than one particle size to be assessed simultaneously. This can similarly be done with the ligaments as sections of the ‘comb’ can have different ligament sizes, but is more difficult with the sheets as the order of sheet failure will be more difficult to control. Despite this, in order to construct this test plan, this has been assumed to be possible.

The preliminary test matrix is given in Table 16. The heat fluxes are those on a 100mm fully catalytic flat faced calibration cylinder.

Test	Type	Particle Size (mm)	Dynamic Pressure (Pa)	Heat Flux (kW/m^2)
1	Ligament	Length 10, Diameter 1 Length 20, Diameter 1	4000	>100
2	Ligament	Length 10, Diameter 1 Length 20, Diameter 1	2000	>100
3	Ligament	Length 10, Diameter 1 Length 20, Diameter 1	1000	>100
4	Sheet	50 x 50 x 1	4000	>100
5	Sheet	50 x 50 x 1	2000	>100
6	Sheet	50 x 50 x 1	1000	>100
7	Particle	30 10	4000	>100
8	Particle	30 10	2000	>100
9	Particle	30 10	1000	>100
10	Particle	3 1	4000	>100
11	Particle	3 1	2000	>100
12	Particle	3 1	1000	>100

Table 16: Preliminary Break-up Campaign Test Matrix

Some flexibility is required in the test campaign, as it may become evident that break-up is either more or less prevalent than expected. Where less break-up than expected is observed, it may be appropriate to run a greater number of tests at higher dynamic pressures as no break-up will be observed where the dynamic pressure is low. There may also be little benefit in running the smaller particle sizes, and these tests could be repurposed to run either larger particles or different ligament/sheet sizes. Conversely, where more break-up is observed, it may be appropriate to run both smaller particle sizes and lower dynamic pressures.

3.2.2 Aluminium Vaporisation Assessment

The experimental set-up for the vaporisation assessment is based on the crucible particle production set-up from the break-up experiments. In these tests, it is intended to assess the vaporisation of the particles post-break-up, and so the size of the particles introduced into the flowfield will be smaller.

The key aspect in these tests shifts from the particles themselves to the amount of aluminium or aluminium oxide vapour that they produce. In order to capture this, optical emission spectroscopy is the preferred diagnostic. However, this will need to be executed in a different manner than is normal at these wind tunnel facilities. The major interest in wind tunnel facilities is usually the gaseous emission from a heat shield into its boundary layer, so the emission spectroscopy is measured along a line through the boundary layer in front of a test sample. This measures the emission in a very precise location.

In this case, the emission is being used as a detector for the vaporisation of aluminium/aluminium oxide particles, and therefore, the highly localised measurements are not of interest. Here, it is important to be able to capture a relatively large volume of the flowfield, and a wide range downstream of the point where the particles are entrained into the flow. The ideal location for the emission spectroscopy is thus

(approximately) along the line of the flow, which suggests that the instrument is set-up downstream of the nozzle exit, pointing in the opposite direction to the flow. It is not clear how diffuse a field can sensibly be captured using these instruments, but the larger a volume which can be assessed, the more particle emission it is possible to detect, which will increase the accuracy of the inference of particle vaporisation.

Whereas the PIV technique which is required for the break-up assessment is sparingly used in plasma wind tunnel testing, and is more common in cold facilities, optical emission spectroscopy is a standard diagnostic in these facilities. Therefore, these diagnostics are well understood, and it is expected that adaptation of this capability is possible.

3.2.2.1 Test Samples

The test samples are simpler in this case, as only the crucible concept is required. In this case, though, the range of required particle sizes are smaller, in order to capture the expected post-break-up size distribution. The interest here is from 20µm to 1mm in diameter, although there may be a pragmatic limit on the smallest size of particle which can be produced in this manner. Some experimentation may be required to assess whether it is sensible to run multiple particle sizes in a single test in this case as the spectroscopy diagnostic will not be able to distinguish the emissions from different particles. Monodisperse distributions are thus preferred at this stage.

3.2.2.2 Test Set-up

The basic set-up for the vaporisation tests is shown in Figure 46. In this case, the PIV is replaced by the emission spectroscopy. It is unlikely that a second emission spectrometer would be available at a single location, but this is desirable and would allow a greater volume of the flow to be assessed, increasing the volume of useful data obtained. Ideally, this would be placed on the other side of the flow from the first spectrometer, also looking along the flow.

Figure 46: Basic Vaporisation Test Set-up

The high-speed camera location is maintained from the break-up tests, as is the location of the first HD camera looking at the release of the particles. The second HD camera is moved downstream and

pointed more in line with the flow to obtain some visible record of the passing particles.

It is possible that some benefit could be obtained from using PIV similarly to its use in the break-up test plan. There are usually some limits to the diagnostics which can be used simultaneously, often driven by the number of viewing windows, but were it possible to run the PIV as well, then this would be advantageous.

3.2.2.3 Test Conditions Derivation

The analysis here follows on from the work in Section 3.2.1.3. The dynamic pressure again forms the proxy for altitude, and the behaviour of the particles at different dynamic pressures is of interest. Added to this is the complication that the flow is significantly hotter and slower (thereby producing a representative heat flux) than would be seen in flight. This changes the balance between the heating and the drag of the particles. As drag is proportional to the square of the velocity, and heating is proportional to the cube, this will act to shift the balance towards drag, rather than heating. This is offset in part due to the higher temperature of the flow, which increases the heating without having a major effect on the drag. This suggests that the heat flux level will be more important for this test campaign.

The average heat flux to the surface of a 10mm particle, as calculated for the fully catalytic surface in Section 2.3.2.1 is given in Figure 47. The equivalent heat flux to a 50mm flat faced fully catalytic reference cylinder is also shown. This suggests that the range of heat fluxes of interest is 25kW/m^2 to 1500kW/m^2, although significant vaporisation is not expected until 85km, or a 300kW/m^2 heat flux.

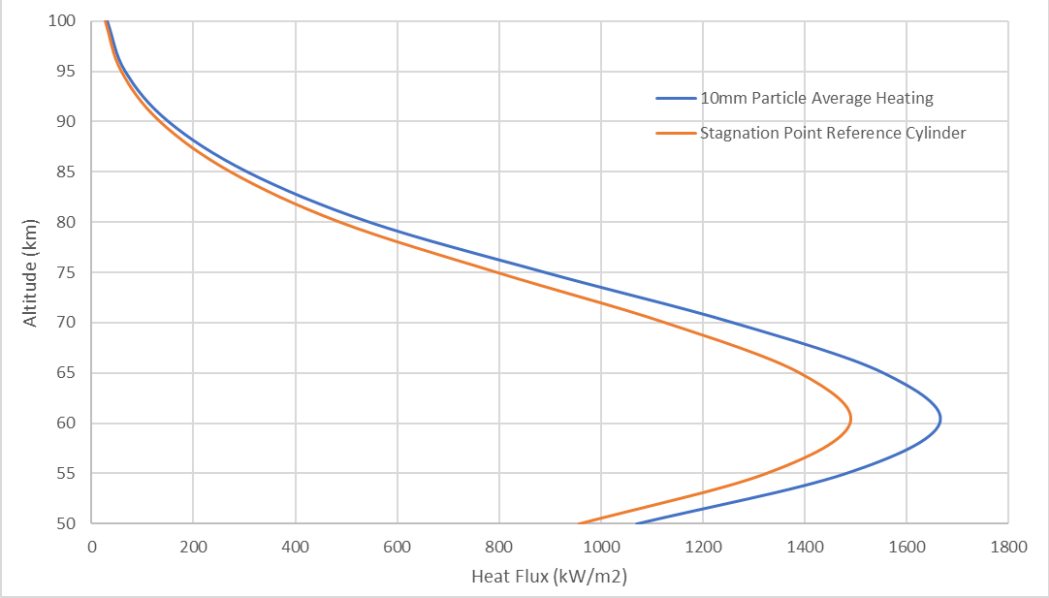

Figure 47: Heat Fluxes on 10mm Particle and Equivalent for Calibration Cylinder

This range of heat fluxes can just be achieved in the L2K facility, although it is significantly more difficult to match the dynamic pressure and the heat flux simultaneously. Given that dynamic pressures can be achieved to 65km altitude, it is suggested to construct the initial test matrix based on heat fluxes and dynamic pressures capturing the 85km to 65km altitude range. Note that L2K is a highly flexible facility, and that it may not be possible to capture this range of heat fluxes with sensible dynamic pressure in other facilities. It is almost certain to be the case that compromises will be required on the test conditions which are facility dependent.

3.2.2.4 Preliminary Test Matrix

Similarly to the break-up campaign, it is assumed that the test campaign is composed of twelve tests. In this case, the particle sizes are monodisperse to avoid complicating the emission spectroscopy results, which are critical to the understanding of the particle vaporisation.

The twelve tests are taken up using four particle sizes at three relevant conditions. As with the break-up campaign, some flexibility is required depending on whether observations of vaporisation can be made at the different conditions. Where no vaporisation is observed, shifting to lower altitude conditions and smaller particles is required. If significant vaporisation is observed, shifting to higher altitude conditions and larger particles will provide a more interesting dataset.

It is almost certain that particles of 1mm and 100µm will be relevant. The selection of larger or smaller particles for the second half of the campaign is dependent upon the results from the break-up campaign. However, for the purposes of the work here, a larger and an intermediate particle size are preliminarily selected.

Test	Particle Size (mm)	Altitude (km)	Dynamic Pressure (Pa)	Heat Flux (kW/m^2)
1	1	85	250	300
2	1	75	1100	800
3	1	65	3400	1400
4	0.1	85	250	300
5	0.1	75	1100	800
6	0.1	65	3400	1400
7	0.3	85	250	300
8	0.3	75	1100	800
9	0.3	65	3400	1400
10	3	85	250	300
11	3	75	1100	800
12	3	65	3400	1400

Table 17: Preliminary Vaporisation Campaign Test Matrix

3.3 Test Planning Conclusions

The construction of a set of plasma wind tunnel tests to investigate the break-up and vaporisation of aluminium particles during destructive spacecraft re-entry has been successfully achieved. Break-up tests can be performed at a set of relevant dynamic pressures on fragmented sheets, ligaments and droplets. Design of the test samples required in order to generate the desired fragments is problematic, but reasonable solutions have been found in all cases.

For the assessment of vaporisation, both the heat flux and the dynamic pressure require capturing, which makes it more challenging to achieve the desired test conditions. It is likely that these conditions will not be perfectly met, so some analysis to extrapolate the test findings to flight will be required to make full use of the data generated.

In both cases, the diagnostics required are different from more standard wind tunnel testing, but existent instrumentation can be applied in order to obtain the desired data. For the break-up testing, this involves use of a PIV system, and for the vaporisation tests, optical emission spectroscopy is required. A unique feature of these tests is that the diagnostics are required downstream of the standard test sample location, which will require significant adaptation of usual diagnostics arrangements in order to observe

the flow significantly downstream of the normal viewing zone.

This exercise has proved to be extremely helpful in outlining the requirements for, and determining the feasibility of, such testing campaigns, and will be useful when contacting facilities to explore the possibility of realising these campaigns.

4 SURVEY OF UK FACILITIES: ATMOSPHERIC RE-ENTRY EMISSION PRODUCTION

The UK facility survey here is targeted at facilities which can potentially improve the understanding of the atmospheric impact of ablation in re-entry, specifically with regard to the species which are deposited into the atmosphere during the ablation process. There are a wide range of potential phenomena of interest in the deposition of spacecraft materials into the atmosphere, and so this survey is not limited to the issue of aluminium particle production, which was the focus of the preceding sections.

The general capabilities for different types of facilities which can be used for high speed aerodynamics and aerothermodynamics, and the phenomena which they could investigate are given in Table 18.

Facility Type	Use	Relevance to Atmospheric Ablation
Shock Tube	High temperature chemistry	Potential gaseous products
Shock Tunnel	High-speed aerodynamics Aerothermodynamic heating	Close to real conditions Aerothermodynamic heating Possible breakup from shock Production of NOx
Hypersonic Wind Tunnel	High-speed aerodynamics	Heating to complex shapes Aerodynamic drag
Plasma Torch/ Arc Heated Wind Tunnel (Plasma Wind Tunnel)	Aerothermodynamic heating Heatshield material testing	Demise of objects Production of realistic fragments Breakup of fragments
Gas Gun	High speed impact	Effect of atmosphere on high speed particles

Table 18: Uses of Relevant Facilities

The aerodynamic and aerothermodynamic facilities are usually used in the design of planetary space missions, either for Earth re-entry or entry into a different atmosphere. The major focus is the survival of a capsule, both in terms of aerodynamic stability and in terms of aerothermodynamic heating. The behaviour of the flow behind the bow shock wave, and the non-equilibrium chemistry in particular, can have an impact on both the pressure and heat flux distributions on the heatshield, affecting both the flight and heating of the capsule. Within Europe, Mars and Titan missions have both been supported by facilities of these types. The gas gun is slightly different in that it primarily used to assess high speed impact into a solid surface, but it can be used to pass particles at high speed through a gaseous environment.

4.1 Physics of Interest

With the focus here being on the production of species which are deposited into the atmosphere, it is worth noting that the target flow regimes of these facilities are the shock layer in front of a stable vehicle, and that is not necessarily the primary interest in this case. The potential zones from which particles originate are from the front (hot) side of a debris fragment as shown in Figure 48. Note that the fragment is almost certain to be tumbling, such that the hot part of the object shifts with time.

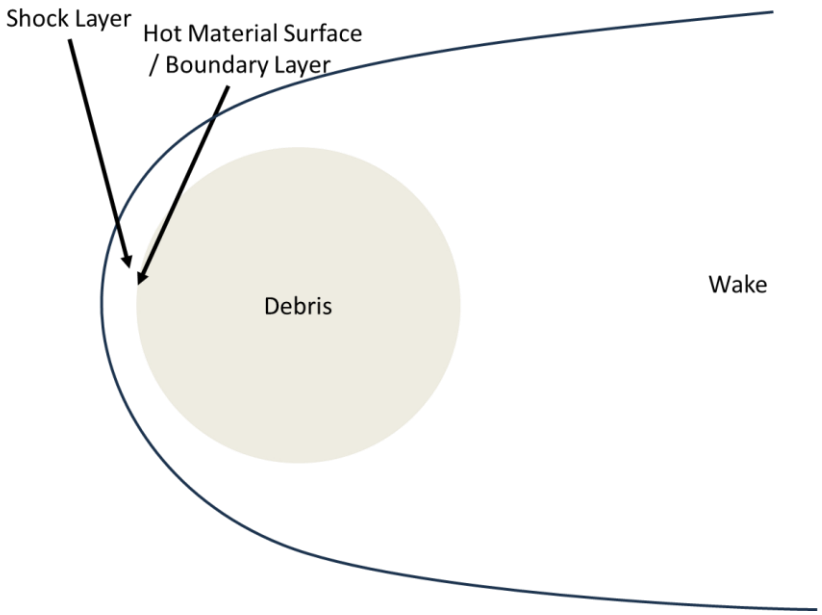

Figure 48: Zones of Interest for Emissions Around Debris Fragment

The majority of the phenomena in terms of the emission from the debris object occur behind the shock wave, where the flowfield and the debris item surface will be hottest. These processes are shown in Figure 49. The production of NOx in the shock layer is a well known phenomenon from meteoroid entry, and is the type of chemical kinetic process which can be investigated with a kinetic shock tube. These processes are very fast, occurring over a timescale of microseconds. The NOx produced is transported into the wake, and although some is expected to decompose, a significant fraction is chemically frozen as the temperature is lower in the wake region. Previous work has estimated that the NOx production is significant (3).

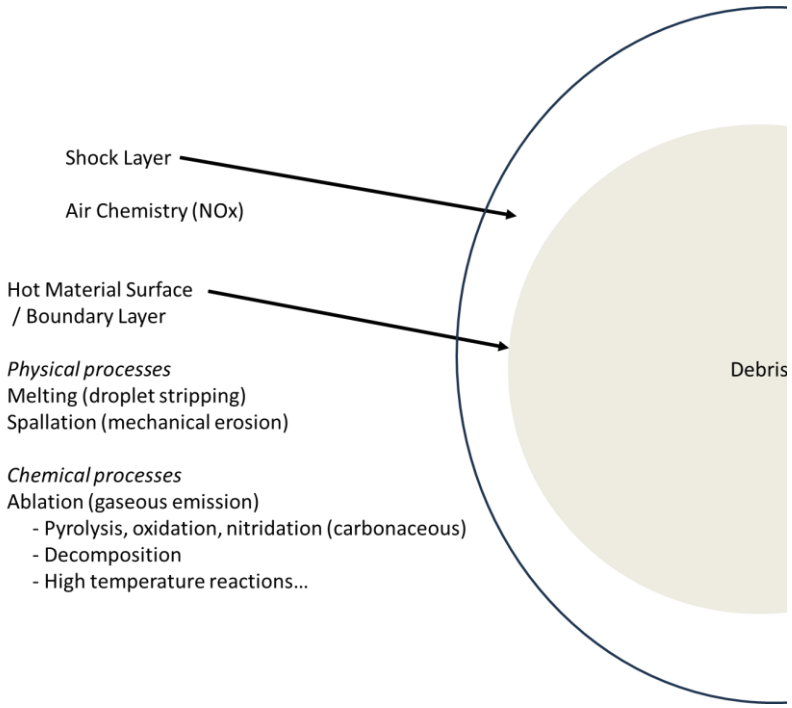

Figure 49: Shock Layer and Material Surface Phenomena

The majority of the phenomena, however, concern the behaviour of the material surface. This is driven

by the heating to object, which is a strong function of its velocity. Thus, the aerodynamic drag is of high importance, which can be assessed for complex component shapes in hypersonic wind tunnels. The heating received by the surface is a more critical quantity to understand, and this is obtained most accurately via shock tunnel experiments. Both the aerodynamics and the aerothermodynamic heating can be obtained by short duration facilities.

The material surface response, however, requires a longer duration facility. To assess this, the facility is required to be able to heat the object for sufficient time that it reaches sufficient temperature for the physical processes (melting, spallation, ablation) to occur. This demonstrates the emissions which can be produced by the debris object, including:

- Liquid droplets from the melting of spacecraft materials
- Solid particles from the break-off of weakened hot material (particularly carbonaceous chars)
- Gaseous emission from pyrolysis of organic materials
- Gaseous emission from oxidation (and nitridation) of surface materials (the main interest is carbon, but some metals are known to have gaseous oxides)
- Emission (solid, liquid or gas) from high temperature reactions of spacecraft materials (not well known)
- Emission (solid, liquid or gas) from the decomposition of spacecraft materials at high temperature (zinc selenide lenses are a good example)

For these processes, the facility of choice is a high enthalpy wind tunnel (often called a plasma wind tunnel) as it is able to produce a hot flow over a significant period of time which can heat the test object. There are two types of high-enthalpy facility mentioned in Table 18. These are inductive plasma torches which generate the heating to the gas via electromagnetic induction, and arc-heated wind tunnels which use an electric arc to heat the gas. Both facilities produce a stream of high energy gas, with the inductive facilities usually being lower speed / higher temperature, and the arc heated facilities being super/hypersonic, but lower temperature. These are the primary facilities of interest for the production of emissions from debris objects.

As discussed at length in the previous parts of this document, the initial release of material from the debris fragment surface does not provide the whole story. For particle deposition, particularly metallic particle deposition, the atmospheric impact is not necessarily driven by the production of particles at the surface of the demising object, but what happens to those particles when they are released into the hypersonic flow.

The important phenomena in the wake are shown in Figure 50. The discussion of the particle heating, deceleration and breakup has been made in Section 2, and there are no facilities which are designed specifically to tackle this regime. There are similarities to meteor / cosmic dust entry in that small particles are heated / decelerated in the atmosphere, but there are significant differences. Firstly, the speed of a re-entering satellite is significantly slower than cosmic dust, and the second is that the particles are released at lower altitudes, meaning that the environment they encounter is significantly harsher than that encountered by particles of similar size entering the atmosphere.

From a material response point-of-view, the timescales involved are much shorter, but still of the order of 0.1-1s, and the high temperature of the particles is critical to their behaviour. This suggests that a high enthalpy facility is again the facility of choice, and this is the facility type used in the test planning of Section 3.

Here, it could be possible to use a light gas gun to assess the particle behaviour as it passes through a static medium, which could provide good data on drag. However, in standard mode, it is unlikely to be possible to heat the gas to the temperatures required to get a reasonable heat flux / vaporisation profile unless the particles are very small. Recent work has suggested that an environment chamber, with gas at pressures of relevance to the atmosphere, could be added within the target chamber (14). This would provide a medium in which the particles could be slowed and heated in a manner relevant to the aluminium particles released from demising spacecraft objects in re-entry. Some work is required to understand the environment densities which are required to obtain sufficient slowing/heating of a high speed particle in the limited distance/time available, and it is not clear whether detection of aluminium vaporisation could be made, but the use of an environment chamber is of high interest. Indeed, this could be a useful complement to the plasma wind tunnel campaigns, particularly for the heating and vaporisation assessment.

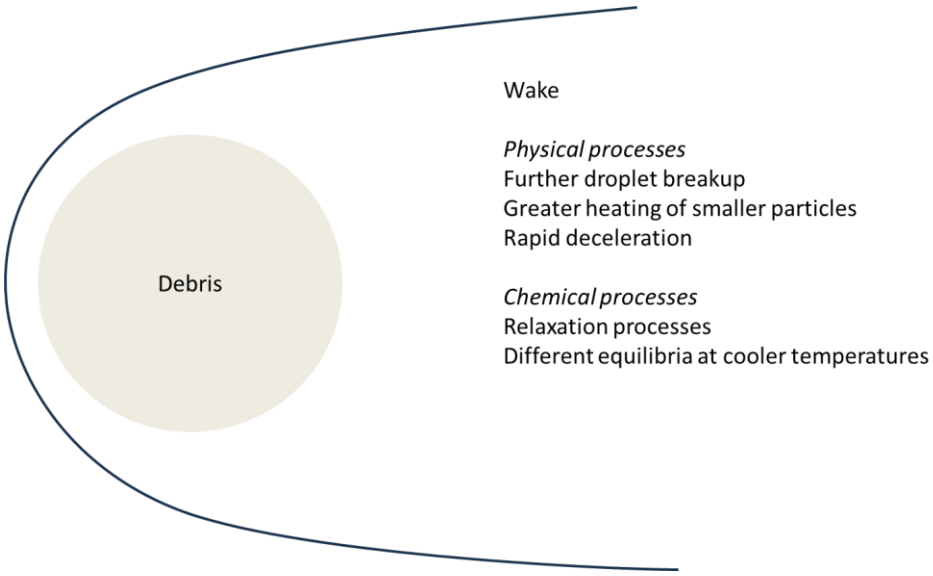

Figure 50: Wake Phenomena

At higher demise altitudes, say above 80km, there is a higher likelihood of chemical non-equilibrium in the wake region, which affects the relaxation processes. Below this altitude, chemical equilibrium is likely due to the higher atmospheric density, and the lower temperatures in the wake region. The non-equilibrium could be investigated using a shock tube, but an improved understanding of the gas phase chemical species expected would be required before this work could be meaningfully undertaken. As relaxation to equilibrium would be expected to be relatively rapidly achieved, there is less value in performing chemical kinetic experiments as these are targeted at understanding the non-equilibrium phenomena.

A summary of the regimes of interest, and the suitable facilities is given in Table 19. A priority for the understanding of the environmental impact of destructive re-entry is also given. Where a test is potentially possible, but there may be difficulties in achieving good results particularly for small particles,

the facility is stated in *italics*.

Phenomenon	Relevant Facilities	Tests	Priority
NOx Production	Shock Tube	Chemical Kinetics	MEDIUM
Surface Melting	Plasma Wind Tunnel	Component Demise	LOW (Many existent tests, not specific to environment impact)
Spallation	Plasma Wind Tunnel	Material Testing Component Demise	MEDIUM (Fewer existent tests)
Pyrolysis	Chemistry Lab	Material Testing	HIGH (Chlorine production)
Gaseous Emission (Component Surface)	Plasma Wind Tunnel	Material Testing Component Demise	LOW (Main emission from particles)
Gaseous Emission (Decomposition)	Chemistry Lab	Heating of Materials in Atmosphere	MEDIUM-HIGH (toxicology)
Component Fragmentation	Plasma Wind Tunnel	Component Demise	LOW (Many existent tests, not specific to environment impact)
Fragment Breakup	Plasma Wind Tunnel *Light Gas Gun*	Particles, Ligaments Sheets in Flow	HIGH (Critical to vaporisation)
Particle Drag	*Shock Tunnel* Light Gas Gun Plasma Wind Tunnel	*Measure Forces* Measure Speed Measure Speed	HIGH (Critical to vaporisation)
Particle Heating	*Shock Tunnel* Light Gas Gun	*Measure Fluxes* Meas. Temperature	HIGH (Critical to vaporisation)
Particle Vaporisation	Plasma Wind Tunnel Light Gas Gun	Measure Emission Measure Emission	HIGH
Chemical Relaxation	*Shock Tube* Chemistry Lab	*Chemical Kinetics* Equilibrium States	MEDIUM (Gaseous emission Expected to drive toxicology)

Table 19: Phenomena, Facilities and Priorities

From this analysis, there are a number of areas which are relevant for the production of potentially harmful emissions from destructive re-entry. The chemical aspects (high temperature material decomposition and pyrolysis) are most appropriately tackled outside the flowfield by gaining an understanding of the potential high temperature chemistry of materials on board spacecraft.

In order to understand the potential for production of very small particles which have a long residence time in the atmosphere, the appropriate facilities are plasma wind tunnels, supported by light gas guns with an environment chamber. The test campaign outlined in Section 3, is appropriate for aluminium particles, and can be supported significantly by light gas gun testing. Indeed, this campaign can be used to develop a methodology for the impact of different particle types on the atmosphere. The assessment of carbon particles is expected to be the next most important species after aluminium.

4.2 Facilities

This section of the work will cover the specific facilities and their capabilities. Notes on the application of these facilities to the experimental needs described in Table 19 will be made. Most of the facilities here are hypersonic facilities with a flowfield, but light gas guns which fire a hypersonic projectile are also considered.

The majority of the hypersonic wind tunnels in the UK are part of the National Wind Tunnel Facility (NWTF) programme (14). This programme covers a wide range of facilities, relevant to environmental flows, automotive and train aerodynamics, and aeronautics. The most relevant facilities to re-entry tend to be the high speed facilities, as these represent the hypersonic flow field around the spacecraft.

There are a wide range of high speed facilities, with test durations from tens of microseconds to tens of minutes. These facilities investigate different aspects of the flowfield and its impact on a target object, and therefore have different uses, which are discussed in the previous section.

The wind tunnel facilities are separated into two sections. The first section is entitled 'hot' facilities where the enthalpy of the flow is such that the heat fluxes generated on the surface of a test object are representative of re-entry conditions. These facilities are relevant to aerothermodynamics. The second section is for 'cold' facilities where the focus is on the high speed aerodynamics.

4.2.1 Hot Hypersonic Facilities

Hot hypersonic facilities are relatively rare, and only a few years ago, there were no such facilities in the UK. Recently, two facilities have been developed at the Osney Thermofluids Institute in Oxford, one a refurbishment of a historic Australian facility, and the other a brand new facility developed with consultancy from the Institute für Raumfahrtsysteme at the University of Stuttgart.

4.2.1.1 T6 Stalker Tunnel (Oxford University)

The T6 Stalker tunnel can run as a reflected shock tunnel, an expansion tunnel, or a shock tube. In shock tunnel mode, it has a 0.15m flow core diameter, a total temperature of up to 5000K and Mach numbers between 6 and 8. The total temperature allows aerothermodynamic heating to be assessed, and this can also be performed on pre-heated surfaces such that the heat flux is measured to a correct surface state.

Hypersonic aerodynamics and heat fluxes can be measured to the test object over the test time of 1-3ms. This is sufficient time for a good assessment of the heating to a particular object, but is not sufficient time to allow a material response to be assessed, even for small particles.

This facility can run test objects either supported or in free flight mode, and has MHz Schlieren imaging at HD resolution, along with high response pressure transducers, high response bespoke thin film gauges and laser optical diagnostics. These are designed to provide precise information over the short test time. The facility specialises in boundary layer stability and transition, supersonic/hypersonic intakes and supersonic combustion for scramjet applications. The laser diagnostics include PLIF (Planar Laser-Induced Fluorescence) which can be used in conjunction with PIV in order to obtain molecular species concentrations. This could be of interest for the detection of aluminium oxide vapour. Also available is LIGTS (Laser Induced Grating Thermal Spectroscopy) which can provide gas phase temperatures.

This is an extremely powerful facility, and is the fastest flow facility in Europe. However, the diagnostic capabilities are likely to be of more interest than the facility itself for the assessment of the environmental impact from destructive re-entry.

4.2.1.2 Osney Plasma Generator (Oxford University)

The Osney Plasma Generator (OSG) is a small plasma wind tunnel which uses a thermal arcjet to heat the flow. The facility produces a continuous high-temperature synthetic air plasma, providing heat fluxes and dynamic pressures which are representative of hypersonic flight and re-entry. A liner traverse system is used to place the items into the flow. Two nozzle exit diameters are available, wither 15mm or 30mm. This limits the size of the test article to approximately 20mm, but this is sufficient for the test of the impact of small particles.

For the test campaigns described in Section 3, this limits the possible size of the samples for the break-up campaign, but it would be expected that the test sample design could be adapted to suit the facility. In particular, the size of sheets would be limited to a 20mm square. This is acceptable to assess sheet break-up, and will provide good data on the particle sizes produced. Indeed, it is likely that this will generate smaller particles, which will provide a worse case for the particle size assessment.

Depending on the conditions used, the Mach number in the flowfield can be up to 3, which means that supersonic flow can be achieved. This provides a more representative heat flux distribution for re-entry studies than is obtained in a subsonic flowfield.

This facility was recently commissioned (2023) and as such it is the first plasma wind tunnel available for use in the UK. Although this is a smaller facility than was in mind when the test campaigns in Section 3 were designed, it provides an opportunity to perform a set of pioneering environmental plasma wind tunnel tests in the UK. As this is a smaller facility. It is also expected that it will be significantly cheaper that using a larger facility. This allows a combination of a reduction in price for the campaign and the potential for a greater number of tests.

For diagnostics, the facility has a number of optical access windows, including the possibility to look along the flow from the end of the chamber (see Figure 51). It is situated within the Osney Thermofluids Institute where there are a number of other hypersonic facilities, and it is expected that the optical diagnostics can be used in this facility. The facility also has standard gauges for measuring a reference heat flux at a test condition, and pitot probes for measuring the stagnation pressure.

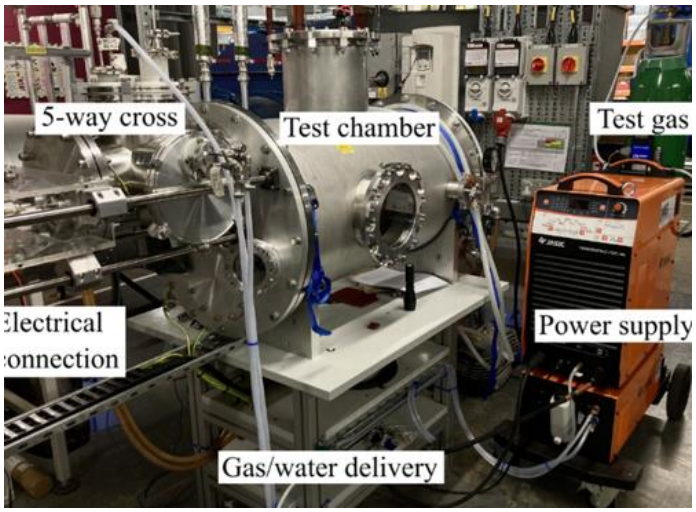

Figure 51: Osney Plasma Generator

Overall, this is expected to be a key UK facility for the investigation of the environmental impact of

ablation in destructive re-entry. Discussion with the facility has revealed the range of dynamic pressure achievable is 1000Pa – 7000Pa, which covers the range for the break-up campaign detailed in Table 16. The 85km condition in the vaporisation campaign of Table 17 is not reachable in the facility, so it is suggested to run a 55km condition instead.

Heat fluxes achievable by the facility are quoted as 1500kW/m^2 on a 15mm diameter probe. Adjusting the figures in Table 17 to this probe size suggests that the heat fluxes required cannot be achieved at the lower altitude conditions. Table 20 gives the desired conditions, with red figures in parentheses noting the conditions which are the best expected to be achieved in the facility.

Test	Particle Size (mm)	Altitude (km)	Dynamic Pressure (Pa)	Heat Flux (kW/m^2)
1	1	85	250 (1000)	500
2	1	75	1100	1450
3	1	65	3400	2500 (1500)
4	0.1	85	250 (1000)	500
5	0.1	75	1100	1450
6	0.1	65	3400	2500 (1500)
7	0.3	85	250 (1000)	500
8	0.3	75	1100	1450
9	0.3	65	3400	2500 (1500)
10	3	85	250 (1000)	500
11	3	75	1100	1450
12	3	65	3400	2500 (1500)

Table 20: Vaporisation Campaign Adapted to Plasma Facility Capability

Even with these compromises, this suggests that the facility is well adapted to the proposed test campaign, and that valuable data on the vaporisation of aluminium particles can be obtained.

4.2.2 Cold Hypersonic Facilities

The majority of hypersonic wind tunnels fall into the classification of cold wind tunnels. These are generally employed for assessing supersonic and hypersonic aerodynamics. It is worth noting that none of the areas of interest identified in Table 19 were directly relevant to these tunnels.

4.2.2.1 Hypersonic Gun Tunnel (Imperial College)

The Imperial College Hypersonic Gun Tunnel is a short duration facility with a nozzle exit diameter of 0.34m. It operates at Mach 9, and can achieve high Reynolds numbers, as well as being able to accommodate long, slender test objects. This makes it an ideal facility for the study of transition and turbulent boundary layers.

With its working gas being nitrogen, and a maximum total temperature of 1150K, and a maximum run time of 20ms, this facility is not ideal for use in assessing the impact of destructive re-entry ablation on the atmosphere. This is an aerodynamics facility, where drag of particular objects could be assessed, and possibly heat flux profiles at significant Mach number could be obtained.

4.2.2.2 High Supersonic Tunnel (Manchester University)

The Manchester University High Supersonic Tunnel (HSST) is a blow-down wind tunnel which can run at Mach 4, 5 or 6. It is a longer duration facility with a maximum run time of 8 seconds. It has been used for aerodynamics of objects, and a 3-component balance sting is available for force measurements.

Transition studies and surface temperature assessments have also been performed.

Flow diagnostics include schlieren imaging, infra-red thermography, pressure and temperature sensitive paints and PIV. Once again, this is primarily an aerodynamics facility, although there is some interest for environmental investigation in the available diagnostic techniques.

4.2.2.3 High Density Tunnel (Oxford University)

The high density tunnel (HDT) is situated in the Osney Thermofluids Institute at the University of Oxford. It can operate as a Ludweig tunnel or a light piston compression heating facility, with test times up to 70ms. This is sufficient for the investigation of unsteady aerodynamic effects, and the Reynolds number is sufficiently high to investigate boundary layer transition.

It operates with air, and has a range of nozzles, allowing flow at Mach 3, 4, 5, 6, 7 and 9. The test flow size is between 0.25m and 0.35m diameter, which allows relatively large models to be tested. Free flight testing is also possible.

The wind tunnel is geared towards boundary layer studies and aerodynamic testing, and is relatively difficult to apply to the needs of environmental impact investigations. The available diagnostics mirror those of the Stalker Tunnel, which suggests that these are available across facilities within the institution. This is of benefit to potential work with the plasma facility.

4.2.2.4 Low Density Tunnel (Oxford University)

The Low Density Tunnel (LDT) is located in the Osney Thermofluids Institute at the University of Oxford, and is significantly different from the other facilities listed here. This is a rarefied flow facility, which is ideal for the investigation of flows at the altitudes of interest for destructive re-entry. The facility can run Knudsen numbers up to 0.3, which is ideal for the investigation of aerodynamics and aerothermodynamics in the rarefied flow regime, where the heating, in particular, is not well understood.

The facility has two nozzles, a contoured Mach 6 nozzle and a conical nozzle which covers the Mach 5-10 range dependent on the distance from the nozzle exit. Aerodynamic coefficients are measured using a magnetic force balance, and aerothermal heating has been measured with thermographic liquid crystals. Free flight tests are also possible, and a set of free flight data acquisition hardware is available.

Diagnostics available include high speed cameras, laser diagnostics and emission spectroscopy. Although this facility is not directly related to the current test campaign being mooted in this activity, it could be an important facility for the investigation of destructive re-entry as there are few facilities worldwide which are capable of running in this highly relevant flow regime.

4.2.2.5 University of Glasgow Facilities

Unfortunately, little data has been unearthed concerning the University of Glasgow facilities, particularly as the supersonic facilities are not part of the NWTF programme. Three facilities have been identified, which are:

- HSS tunnel: this is a blow down wind tunnel which can run up to Mach 5. Diagnostics include pressure sensitive paint and PIV.

- Shock tube: this is a supersonic shock tube, running only to Mach 2, and as such is less interesting for re-entry flows than other, faster, shock tube facilities.
- Shock tunnel: this has a more relevant speed range of Mach 5 to Mach 7, and a 10ms run time. The diagnostics appear to be shared with the HSS tunnel.

As with the similar facilities considered above, there is a limit to the relevance of these facilities to the investigation of environmental impact from destructive re-entry.

4.2.3 Light Gas Guns

Light gas guns have been used to fire small projectiles at very high velocity in order to investigate the behaviour of cosmic dust. Although primarily used in hypervelocity impact studies, recent developments have included placing an environment chamber with a higher pressure gas within the target chamber. This, when penetrated by the particle, can simulate the passage of a hypervelocity particle through an atmospheric medium. This development has significant potential for the investigation of the fate of aluminium particles produced in the re-entry demise process, and suggests that a light gas gun could be used complementarily to investigate the potential vaporisation of small particles. As many hypervelocity impact experiments are already performed with aluminium projectiles of relevant sizes, this makes gas guns a useful addition to the set of facilities which can be used to investigate re-entry ablation.

4.2.4 Light Gas Gun (University of Kent)

The two-stage light gas gun at the University of Kent is shown in Figure 52. The gun can fire single projectiles from 0.1mm to 3mm diameter, and multiple (buck-shot) projectiles from 1-400 microns diameter. These shots can be from 300m/s to 7.5km/s, although the highest velocities may not be accessible for the largest particle sizes. The target can be heated or cooled.

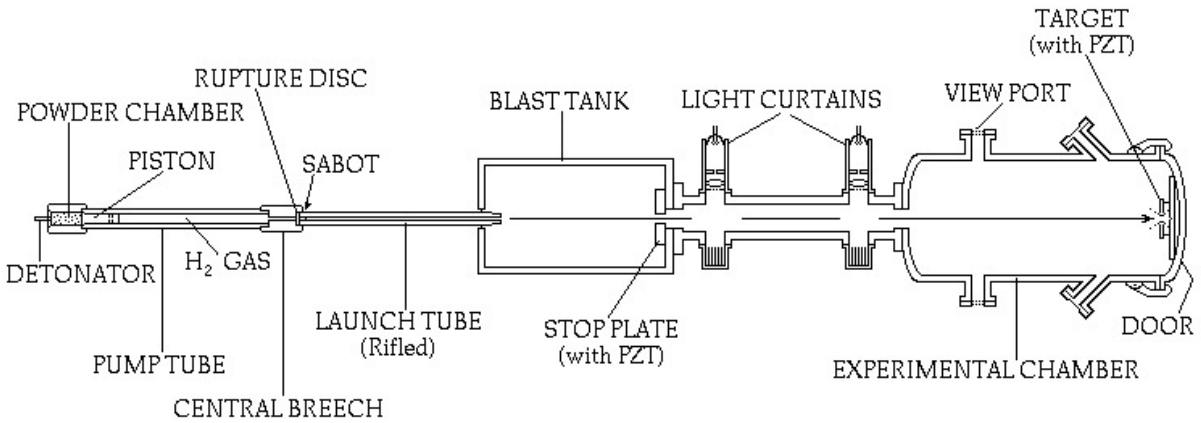

Figure 52: Kent Light Gas Gun Schematic

The quoted minimum pressure in the chamber is 50Pa, with the environment chamber being able to reach pressures of 2 bar. 50Pa is approximately the pressure at 55km, which suggests that lower pressures would be preferred for a test campaign on atmospheric ablation.

4.2.5 All-Axis Light Gas Gun (Open University)

The All-Axis Light Gas Gun is a two-stage light gas gun, which is of a very similar design to the Kent

facility. It has the additional capability of being able to be oriented in any direction for firing, with vertical firing being beneficial for the study of hypervelocity impact into regoliths.

Diagnostic capabilities include laser intervalometer projectile velocimetry, high speed cameras and a high speed pyrometer. This suggests that both the speed and the velocity of a projectile could be measured.

Single particles from 0.5mm to 4.5mm diameter are regularly used, with buck-shot type firings available for particles from 1-500 microns. The maximum velocity of the facility is approximately 7km/s, and the minimum pressure which can be achieved in the gun is 20Pa, which is equivalent to about 60km altitude, which brings it close to the region of interest for the test campaign. This lower pressure is of interest for the higher altitudes in the proposed test campaign. The vaporisation campaign suggested in Table 17 is reproduced here as Table 21, with the heat flux column replaced by particle velocity.

As was done for the plasma facility, the conditions which cannot be achieved are noted by placing a red figure in parentheses for the best achievable condition. The dynamic pressures are high, which will result in faster deceleration of the particles than would be seen in re-entry.

Test	Particle Size (mm)	Altitude (km)	Dynamic Pressure (Pa)	Velocity (m/s)
1	1	85	250 (5700)	7700 (7000)
2	1	75	1100 (5700)	7300 (7000)
3	1	65	3400 (4900)	6500
4	0.1 (buck-shot)	85	250 (5700)	7700 (7000)
5	0.1 (buck-shot)	75	1100 (5700)	7300 (7000)
6	0.1 (buck-shot)	65	3400 (4900)	6500
7	0.3	85	250 (5700)	7700 (7000)
8	0.3	75	1100 (5700)	7300 (7000)
9	0.3	65	3400 (4900)	6500
10	3	85	250 (4200)	7700 (6000)
11	3	75	1100 (4200)	7300 (6000)
12	3	65	3400 (4200)	6500 (6000)

Table 21: Vaporisation Test Plan for Light Gas Gun

It should be noted, however, that a higher deceleration of the particles may be required in order to assess the vaporisation as the particles need to be heated sufficiently in a very short timescale, and this is better achieved in a denser atmosphere. Therefore, it is expected that the above campaign outline would be augmented with higher pressure tests in order to validate numerical models which can be extrapolated to re-entry conditions.

4.3 Other Useful Facilities/Experts

4.3.1 High Temperature Chemistry Expertise

In Table 19, a number of phenomena have been suggested to be performed in standard chemistry laboratories. For many materials, the decomposition or oxidation reactions at high temperature are reasonably well known, and application to reactive element (such as chlorine) or toxic (such as selenium) may be achieved by bringing together chemists and destructive re-entry specialists without need for further testing. However, this can only be assessed once the different experts are assembled.

4.3.2 Thermal Spray Expertise

Specifically for the aluminium vaporisation assessment, it has been noted that there is significant research in the field of thermal sprays, which are sprays of small metallic droplets which are used to produce coatings. This field is of practical interest to experimentation with hot metallic particles, and a plume temperature and velocity can be measured using the appropriate instrumentation. There are also instruments which will measure individual particle velocities and temperatures.

The individual particle measurements are of particular interest, but the leading instrument, the DPV Evolution, focusses on a very small volume within a spray. For the purposes of an aluminium particle vaporisation experiment, it is likely to be extremely difficult to ensure that particles pass through the particular small volume, and expertise on the application of these diagnostic systems to the specific case of a small number of particles would be useful.

It is also worth noting that the range of velocities and temperatures are likely to be different in thermal sprays. The diagnostic measurements are up to 1200m/s, which is well below what is needed for a gas gun, but may be marginal for a Mach 3 plasma facility. The temperature measurements are expected to be relevant as they are above 1050^0C, and are optical emission based. Interestingly, the particle diameters measured are from 5-300µm, and although this covers some of the range of interest, there will certainly be interest in larger particles as these are produced in destructive re-entry.

4.4 Application to Aluminium Particle Ablation Assessment

The available UK facilities have been reviewed to assess their usefulness for the investigation of environmental impact from atmospheric ablation in destructive re-entry. The most relevant facilities for the specific problem of aluminium vaporisation are the plasma torch at the University of Oxford and a light gas gun. The responsiveness of the Open University has resulted in the preference of the all-axis light gas gun for the mooted test programme.

In order to generate the necessary data, it is proposed to run the test programme in two stages. As these tests will be innovative in nature, there is an exploratory aspect to the work, which means that an initial campaign in each facility type will provide a significant amount of learning to be applied in the subsequent campaign. As there is significant work involved, and time is required to apply the learning from the first campaign, it is proposed to perform this over approximately an 18 month period, requiring funding in two financial years.

Investigation of the costs of the facilities suggests that the programme could be split into two equal parts, with a total cost of approximately £250,000, equating to £125,000 for each of two financial years. The separate costs for the facilities are given in Table 22.

Organisation	Role	Year 1	Year 2	Total Cost
Belstead Research	Lead, Analysis, Application	£45,000	£45,000	£90,000
Oxford University	Plasma Torch Testing	£60,000	£60,000	£120,000
Open University	Light Gas Gun Testing	£20,000	£20,000	£40,000
TOTAL		**£125,000**	**£125,000**	**£250,000**

Table 22: Approximate Costs for Aluminium Particle Test Campaigns

Although the costs here do not include thermal spray expertise, it is expected that this expertise will be spun-in through a set of conversations. If necessary, a small consultancy could be considered.

This suggests that a ground-breaking test campaign based on the analysis of Section 2, and approximating the ideal test campaign of Section 3, can be constructed using a set of UK facilities. This would put the UK at the forefront of research into the understanding of the products from destructive re-entry which could have an atmospheric impact.

5 BIBLIOGRAPHY

1. *Plasma wind tunnel demisability testing of spacecraft equipment.* **Beck, J, et al.** Monopoli : s.n., 2019. International Conference on Flight Vehicles, Aerothermodynamics and Re-entry (FAR).

2. *Improved representation of destructive spacecraft re-entry from analysis of high enthalpy wind tunnel tests of spacecraft equipment.* **Beck, J, et al.** 2019, Acta Astronautica, Vol. 164, pp. 287-296.

3. *Aerothermodynamic assessment of atmospheric emissions from re-entry demise.* **Beck, J, et al.** Monopoli : s.n., 2019. 1st International Conference on Flight Vehicles Aerothermodynamics and Re-entry missions (FAR).

4. **Beck, J and Holbrough, I.** *Statistical database of re-entry casualty risk from historic upper stages.* 2025. BRL report PR0109-D01.

5. *Assessment of re-entry survivability of aluminium oxide with different nanostructures considering surface catalytic heat transfer.* **Park, S, Yang, Y and Kim, I.** 2024, Case studies in thermal engineering, Vol. 55.

6. *Dynamics of secondary drop breakup - a rate controlling process in dense sprays.* **Faeth, G.** Zaragoza : s.n., 2002. ILASS-Europe.

7. *Flow induced breakup of drops and Bubbles.* **Jain, S.** 2017. arXiv:1701.06157v1.

8. *Secondary breakup of a drop at moderate Weber numbers.* **Jain, M, et al.** 2015, Proc. Roy. Soc. Series A, Vol. 471, pp. 1-25.

9. *A chemical model of meteoric ablation.* **Vondrak, T, et al.** 2008, Atmospheric chemistry and physics, Vol. 8, pp. 7015-7031.

10. **Lide, D.** *CRC Handbook of Chemistry and Physics.* s.l. : Taylor & Francis, 2007.

11. **Aluminium Oxide Evaporation Process Notes.** ***Kurt J. Lesker Company.*** **[Online] https://www.lesker.com/newweb/deposition_materials/deposition-materials-notes.cfm?pgid=al6#:~:text=Aluminum%20oxide%2C%20or%20more%20commonly,density%20of%203.97%20g/cc..**

12. *Thermal laser evaporation of elemental metal sources in oxygen.* Kim, DY, Smart, T and Majer, L. 2022, J. Applied Physics, Vol. 132.

13. *A study of wire break-up and in-flight particle behaviour during wire frame spraying of aluminium.* Lunn, G, Riley, M and McCartney, D. 2017, J. Therm. Spray Tech., Vol. 26, pp. 1947-1958.

14. Beck, J, et al. *Characterisation of materials and structures under re-entry conditions: final report.* 2023. BRL report PR00093/D45.

15. *Simulating atmospheric alteration of micrometeorites using a two stage light gas gun.* Alesbrook, L, et al. Berlin : s.n., 2018. European Planetary Science Congress.

16. National Wind Tunnel Facility. ***National Wind Tunnel Facility.*** **[Online] www.nwtf.ac.uk.**